The American Journal of Human Genetics, Volume *103*

Supplemental Data

Recessive *DNAH9* Loss-of-Function Mutations Cause Laterality Defects and Subtle Respiratory Ciliary-Beating Defects

Niki T. Loges, Dinu Antony, Ales Maver, Matthew A. Deardorff, Elif Yýlmaz Güleç, Alper Gezdirici, Tabea Nöthe-Menchen, Inga M. Höben, Lena Jelten, Diana Frank, Claudius Werner, Johannes Tebbe, Kaman Wu, Elizabeth Goldmuntz, Goran Čuturilo, Bryan Krock, Alyssa Ritter, Rim Hjeij, Zeineb Bakey, Petra Pennekamp, Bernd Dworniczak, Han Brunner, Borut Peterlin, Cansaran Tanidir, Heike Olbrich, Heymut Omran, and Miriam Schmidts

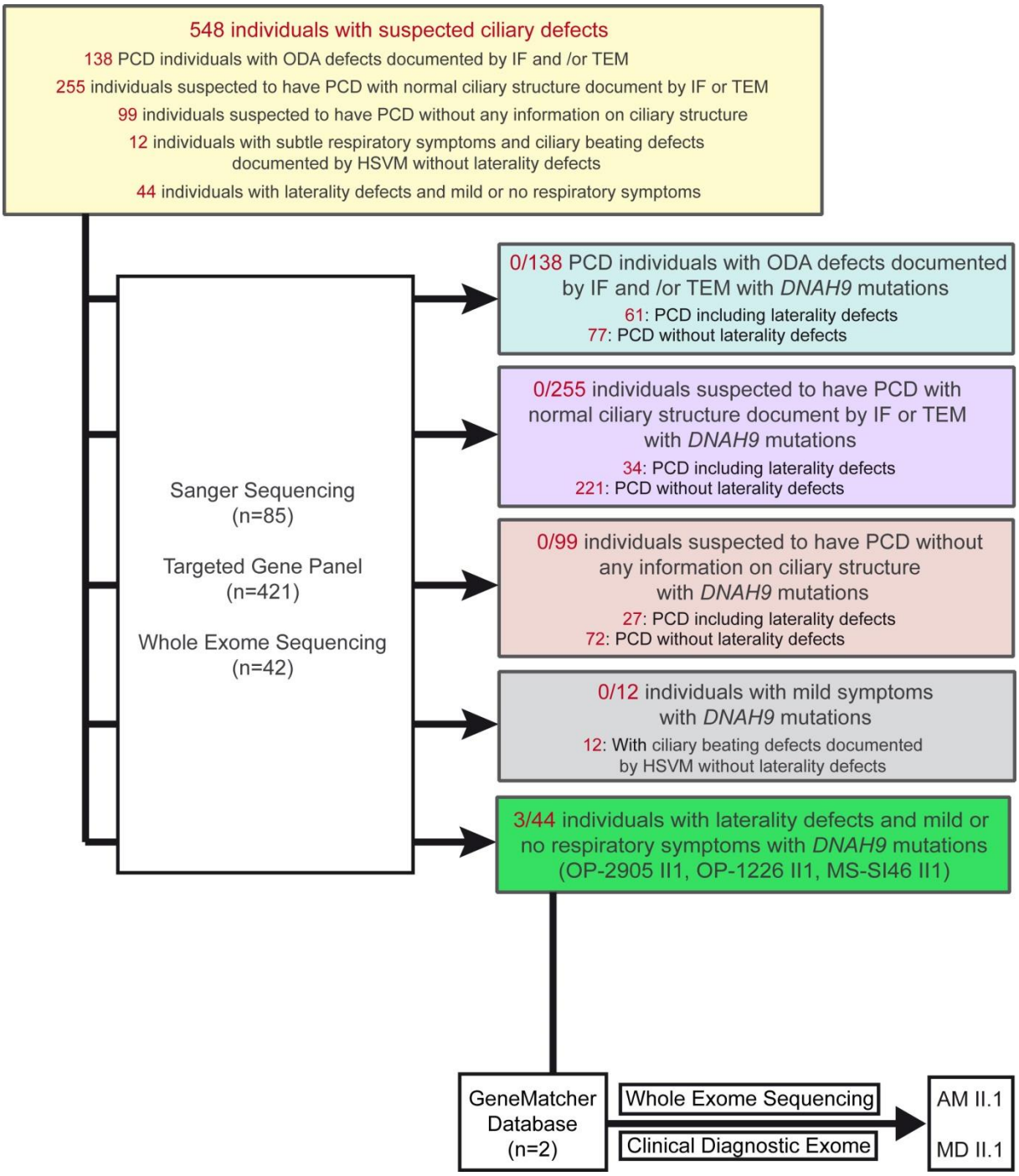

Figure S1. Consort style diagram of present study. The study included 548 individuals with suspected ciliary defects and *DNAH9* was sequenced with Sanger Sequencing and different Next Generation Sequencing methods. Methods are described in the supplemental methods. An overview of the genes included in the gene panel is shown in Table S1. In total, five individuals with loss-of-function mutations in *DNAH9* with laterality defects and mild or no respiratory symptoms were identified. Individuals AM II.1 and MD II.1 were identified in the GeneMatcher Database. HSVM: High Speed Video Microscopy; IF: Immunofluorescence analyses; ODA: Outer Dynein Arm; PCD: Primary Ciliary Dyskinesia; TEM: Transmission Electron Microscopy

A

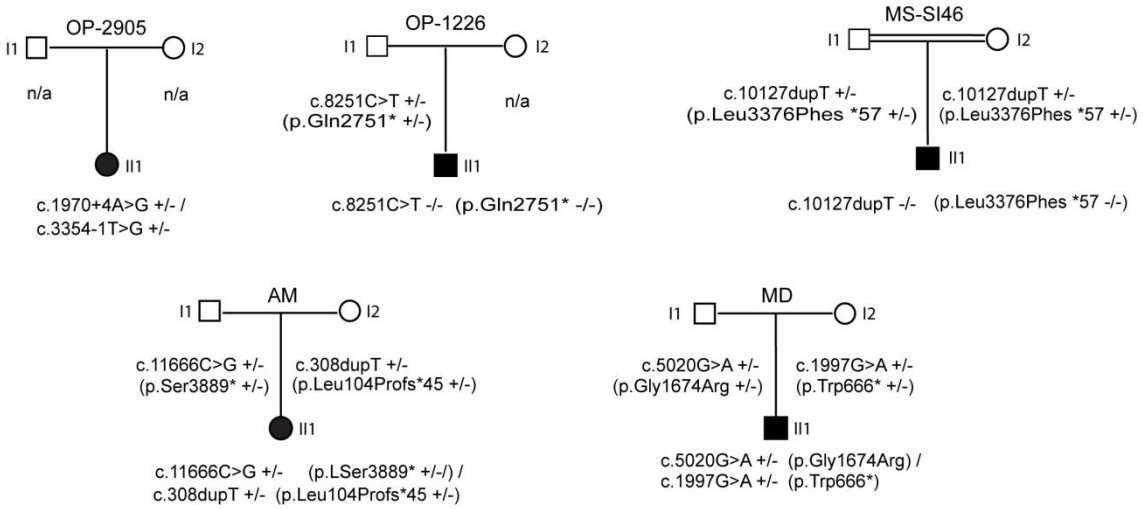
OP-2905
I1
I2
n/a
n/a
II1
c.1970+4A>G +/- /
c.3354-1T>G +/-
OP-1226
I1
I2
c.8251C>T +/-
(p.Gln2751* +/-)
n/a
II1
c.8251C>T -/- (p.Gln2751* -/-)
MS-SI46
I1
I2
c.10127dupT +/-
(p.Leu3376Phes *57 +/-)
c.10127dupT +/-
(p.Leu3376Phes *57 +/-)
II1
c.10127dupT -/- (p.Leu3376Phes *57 -/-)
AM
I1
I2
c.11666C>G +/-
(p.Ser3889* +/-)
c.308dupT +/-
(p.Leu104Profs*45 +/-)
II1
c.11666C>G +/- (p.LSer3889* +/-/) /
c.308dupT +/- (p.Leu104Profs*45 +/-)
MD
I1
I2
c.5020G>A +/-
(p.Gly1674Arg +/-)
c.1997G>A +/-
(p.Trp666* +/-)
II1
c.5020G>A +/- (p.Gly1674Arg) /
c.1997G>A +/- (p.Trp666*)

B

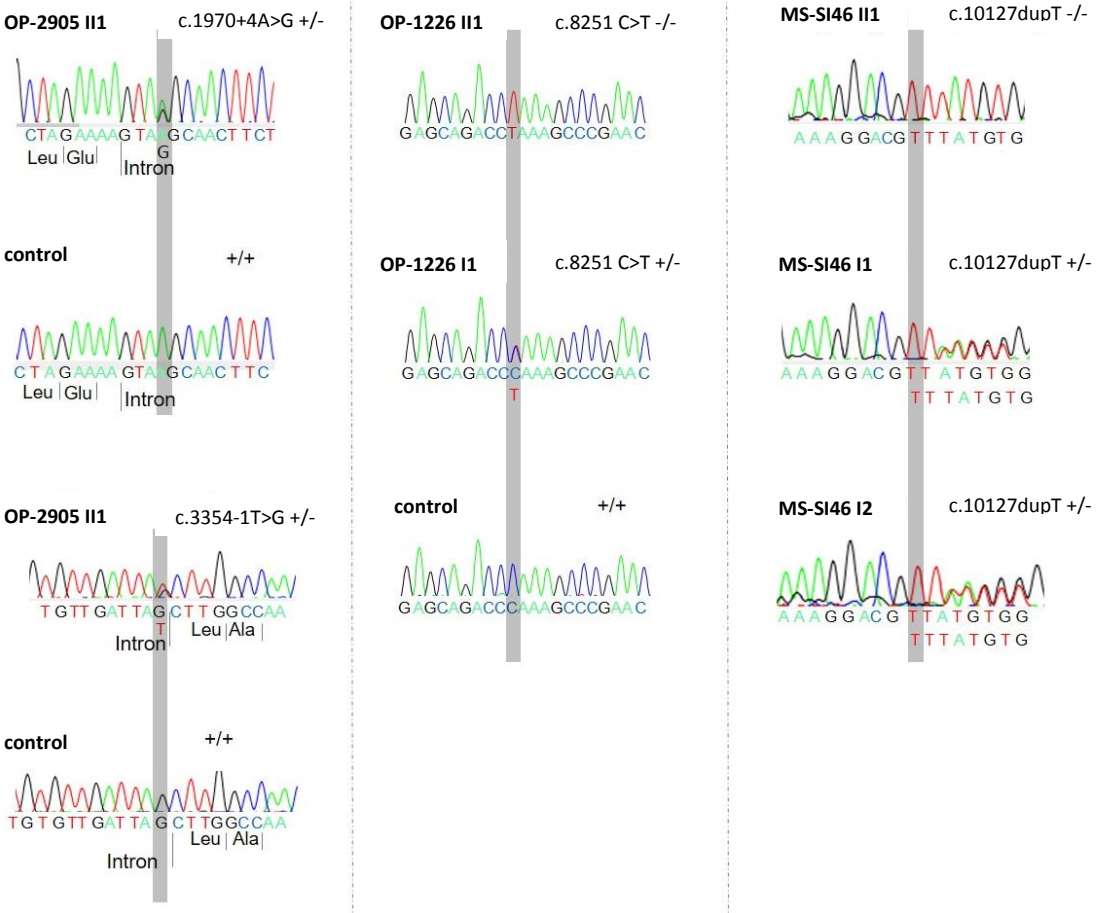
OP-2905 II1
c.1970+4A>G +/-
Leu Glu
Intron
control
+/+
OP-2905 II1
c.3354-1T>G +/-
Intron
Leu Ala
control
+/+
Intron
Leu Ala
OP-1226 II1
c.8251 C>T -/-
OP-1226 I1
c.8251 C>T +/-
control
+/+
MS-SI46 II1
c.10127dupT -/-
MS-SI46 I1
c.10127dupT +/-
MS-SI46 I2
c.10127dupT +/-

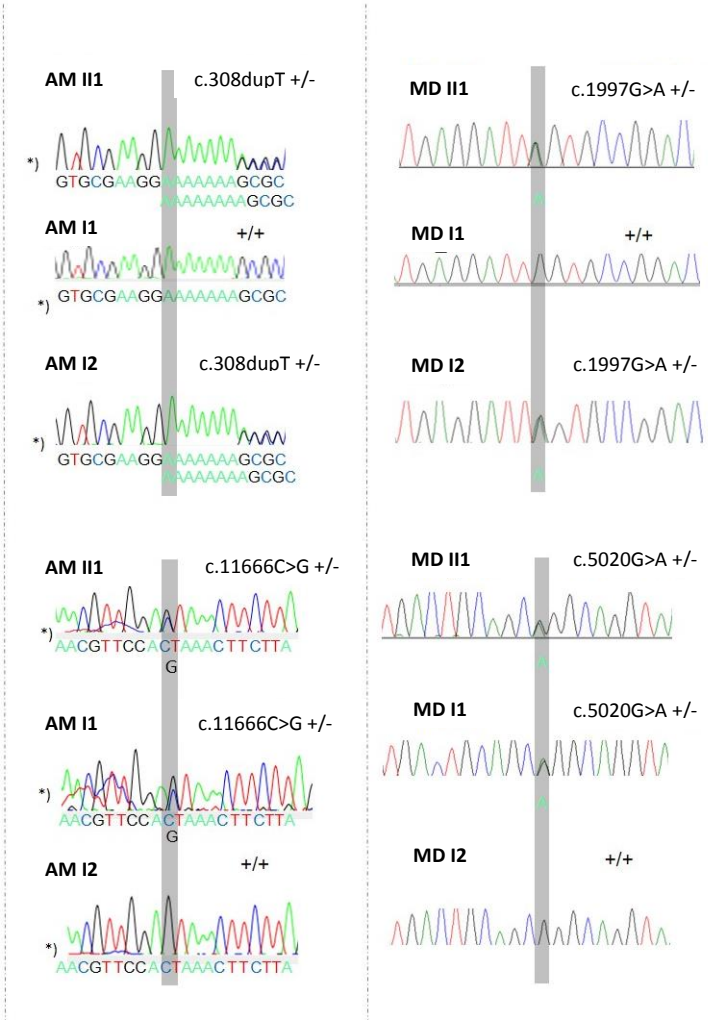

Figure S2. Results of the mutational analyses in *DNAH9*. All variants in *DNAH9* identified by different Next Generation Sequencing methods were confirmed by Sanger sequencing. (A) Pedigrees of affected families with segregation patterns and (B) chromatograms from Sanger sequencing.*) indicates reverse sequencing direction. In total, we identified eight different variants in *DNAH9* in five individuals from five independent families of which one is a missense allele affecting a highly conserved amino acid (c.5020G>A, p.Gly1674Arg) while the seven remaining represent potentially null alleles (c.1970+4A>G; c.3354-1G>T; c.8251C>T, p.Gln2751*; c. 10127dupT, p.Leu3376Phefs*57; c.308dupT, p.Leu104Profs*47; c.11666C>G, p.Ser3889* and c.1997G>A, p.Trp666*).

Interpreted Data

This table shows only relevant results related to the mutation position and context.

Predicted signal	Prediction algorithm	cDNA Position	Interpretation
Broken WT Donor Site	1 - HSF Matrices	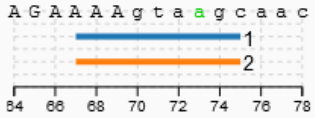	Alteration of the WT donor site, most probably affecting splicing.
	2 - MaxEnt		

Raw Data Tables

In the tables below, positions in sequence for the 5' intron are labeled as negative and as positive for the 3' intron.
Variations in the tables below are noted in colored boxes, according to the following scale:

Site broken	0% - 25% variation	26% - 50% variation	51% - 75% variation	76% - 100% variation	New site<

Potential Splice Sites | Potential Branch Points | Enhancer motifs | Silencer motifs | Other splicing motifs

HSF Matrices

Sequence Position	cDNA Position	Splice site type	Motif	New splice site	Wild Type	Mutant	If cryptic site use, exon length variation	Variation (%)
162	62	Acceptor	CTAGAAAAgtaagc	ctagaaaagtagGC	42.2	71.15	NA	New site +68.6
167	67	Donor	AAAgtaagc	AAAgtaggc	86.29	77.95	78	-9.67

MaxEnt

Threshold values:
5' Motif: 3 3' Motif: 3

Sequence Position	cDNA Position	5' Motif					3' Motif				
		Ref Motif	Ref Score	Mut Motif	Mut Score	Variation (%)	Ref Motif	Ref Score	Mut Motif	Mut Score	Variation (%)
167	67	AAAgtaagc	7.31	AAAgtaggc	5	-31.6					

Interpreted Data

This table shows only relevant results related to the mutation position and context.
The mutation occurs in the late intronic positions, the following table show results of acceptor splice sites that could be affected by the mutation

Predicted signal	Prediction algorithm	cDNA Position	Interpretation
Broken WT Acceptor Site	1 - HSF Matrices 2 - MaxEnt	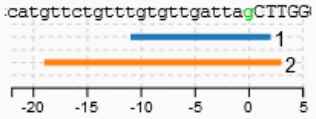	Alteration of the WT acceptor site, most probably affecting splicing.

Raw Data Tables

In the tables below, positions in sequence for the 5' intron are labeled as negative and as positive for the 3' intron.
Variations in the tables below are noted in colored boxes, according to the following scale:

Site broken	0% - 25% variation	26% - 50% variation	51% - 75% variation	76% - 100% variation	New site<

Potential Splice Sites | Potential Branch Points | Enhancer motifs | Silencer motifs | Other splicing motifs

HSF Matrices

Sequence Position	cDNA Position	Splice site type	Motif	New splice site	Wild Type	Mutant	If cryptic site use, exon length variation	Variation (%)
89	-12	Acceptor	tgtgttgattagCT	tgtgttgattatCT	72.67	43.72	0	WT site broken -39.84

MaxEnt

Threshold values:
5' Motif: 3 3' Motif: 3

Sequence Position	cDNA Position	5' Motif					3' Motif				
		Ref Motif	Ref Score	Mut Motif	Mut Score	Variation (%)	Ref Motif	Ref Score	Mut Motif	Mut Score	Variation (%)
81	-20						gttctgtttgtgttgattagCTT	4.41	gttctgtttgtgttgattatCTT	-4.18	-194.78

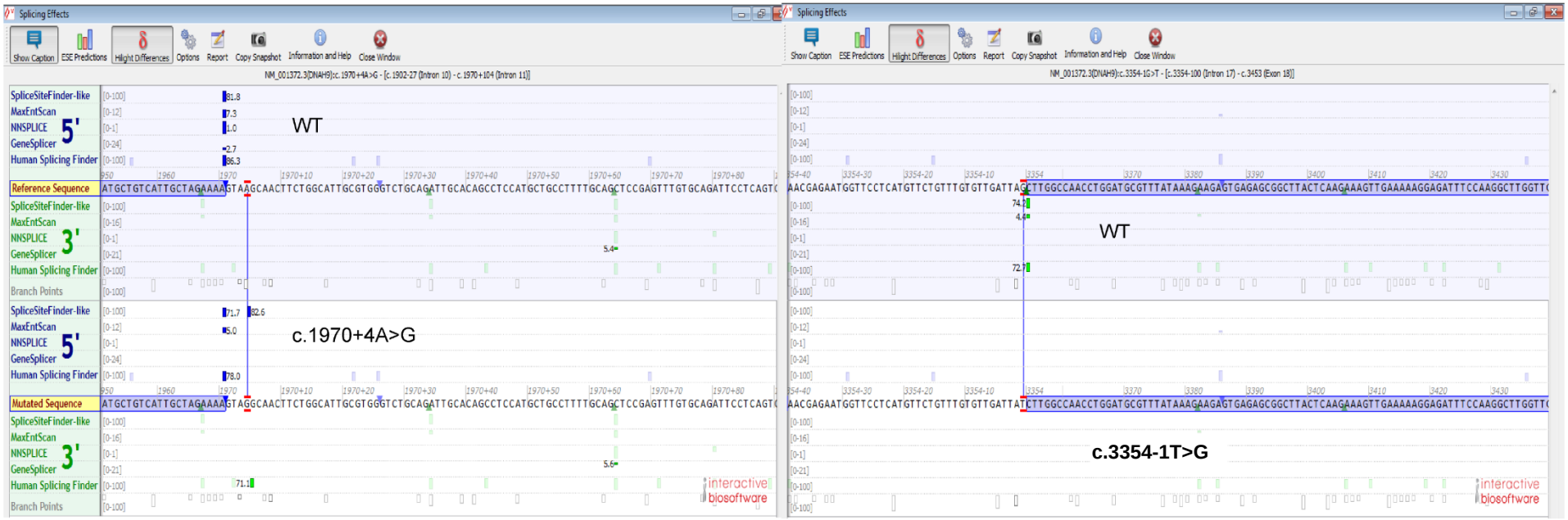

Figure S3. Prediction of the pathogenicity of the *DNAH9* splice sites variants identified in OP-2905 II1. The variant c.1970+4A>G affecting the donor splice site of *DNAH9* exon 11 is predicted to change this donor splice site and most probably affect splicing. The variant c.3354-1G>T affects the acceptor splice site of *DNAH9* exon 18 and likewise probably disturbs splicing. Predictions were performed using the Human Splicing Finder (www.umd.be/HSF/) and Alamut interactive biosoftware.

Species	Protein		match	aa	alignment
H.sapiens	DNAH9	NP_001363.2	identical	1674	Y V A F S E P C D C S **G** Q V E I W L
H.sapiens mutated	DNAH9	NP_001363.2	-	1674	Y V A F S E P C D C S **R** Q V E I W L
M.musculus	DNAH9	NP_001093103.1	identical	1672	Y V A F S E A C D C S **G** Q V E I W L
G.gallus	DNAH9 predicted	XP_415585.4	identical	1568	Y V A F S E P C D C S **G** Q V E I W L
D.rerio	Dnah9	XP_515585.4	identical	1709	Y V P F S Q P C V C E **G** Q A EC W L
X.tropicalis	Dnah9 predicted	XP_017953321.1	identical	1518	Y V P F N E P C D C S **G** Q V ET W L
D.melanogaster	Dhc 93AB, isoform B	NP_524424.2	identical	1673	L A S I R **G** P V EV W L
C.reinhardtii	DHCβ	XP_001695126.1	identical	1722	V V E F V E D C S C D **G** P V EV W L

Figure S4. Analysis of the evolutionary amino acid conservation in DNAH9. ClustalW analyses of the human amino acid position 1674 found to be mutated in individual MD II.1 show evolutionary conservation throughout species.

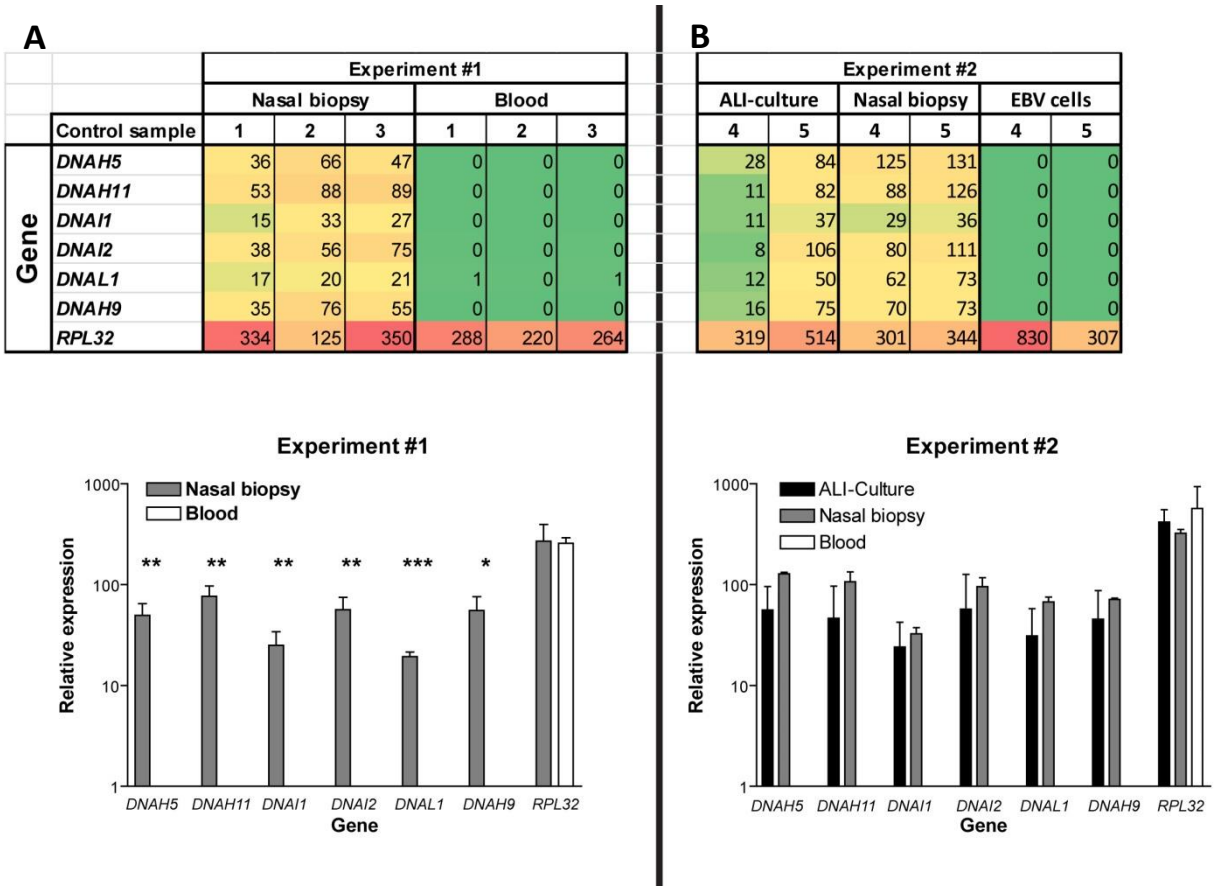

Figure S5. Tissue-specific expression profiles of known genes encoding for components of the outer dynein arm (ODA) complex and *RLP32 (60S ribosomal protein L32)* as a housekeeping gene. Raw RNA-seq data were normalized against *PPIH* (*peptidylprolyl isomerase H*). (A) The genes encoding ODA components are upregulated in native material of nasal brushing biopsies compared to blood cells (n = 3). (B) A similar upregulation of genes encoding ODA components are observed in ALI-cultured epithelial nasal cells and in nasal brush biopsies compared to EBV-cells (immortalized lymphocytes) (n = 2). *RPL32* shows a high expression in all analyzed tissues. Two independent experiments (experiment #1 and #2) with samples from respectively 3 and 2 control individuals (samples 1-5) were performed. All statistical analyses were performed using GraphPad Prism 3 (GraphPad Software Inc., San Diego, CA) and IBM SPSS Statistics 25 (IBM, Armonk, NY). The results are provided as mean ± Standard Deviation. Single comparison between nasal brushing biopsies and blood in experiment #1 were analyzed using one-tailed Student's t-test with Bonferroni-correction. p values < 0.05 were considered significant. *p < 0.05, ** p < 0,01, *** p < 0,001. Standard Deviations for Experiment #1: *DNAH5*=±15.2; *DNAH11*=±20.5; *DNAI1*=±9.2; *DNAI2*=±18.5; *DNAL1*=±2.1; *DNAH9*=±20.5; *RPL32*=±125.5 (nasal biopsy, NB) and ±34.5 (blood). Standard Deviations for Experiment #2: *DNAH5*=±40.1 (ALI-culture, AC) and ±4.0 (NB); *DNAH11*=±50.1 (AC) and ±27.1 (NB); *DNAI1*=±17.7 (AC) and ±5.5 (NB); *DNAI2*=±69.4 (AC) and ±21.9 (NB); *DNAL1*=±26.1 (AC) and ±7.3 (NB); *DNAH9*=±41.9 (AC) and 2.0 (NB); *RPL32*=±137.9 (AC), ±30.4 (NB) and ±369.8 (EBV cells).

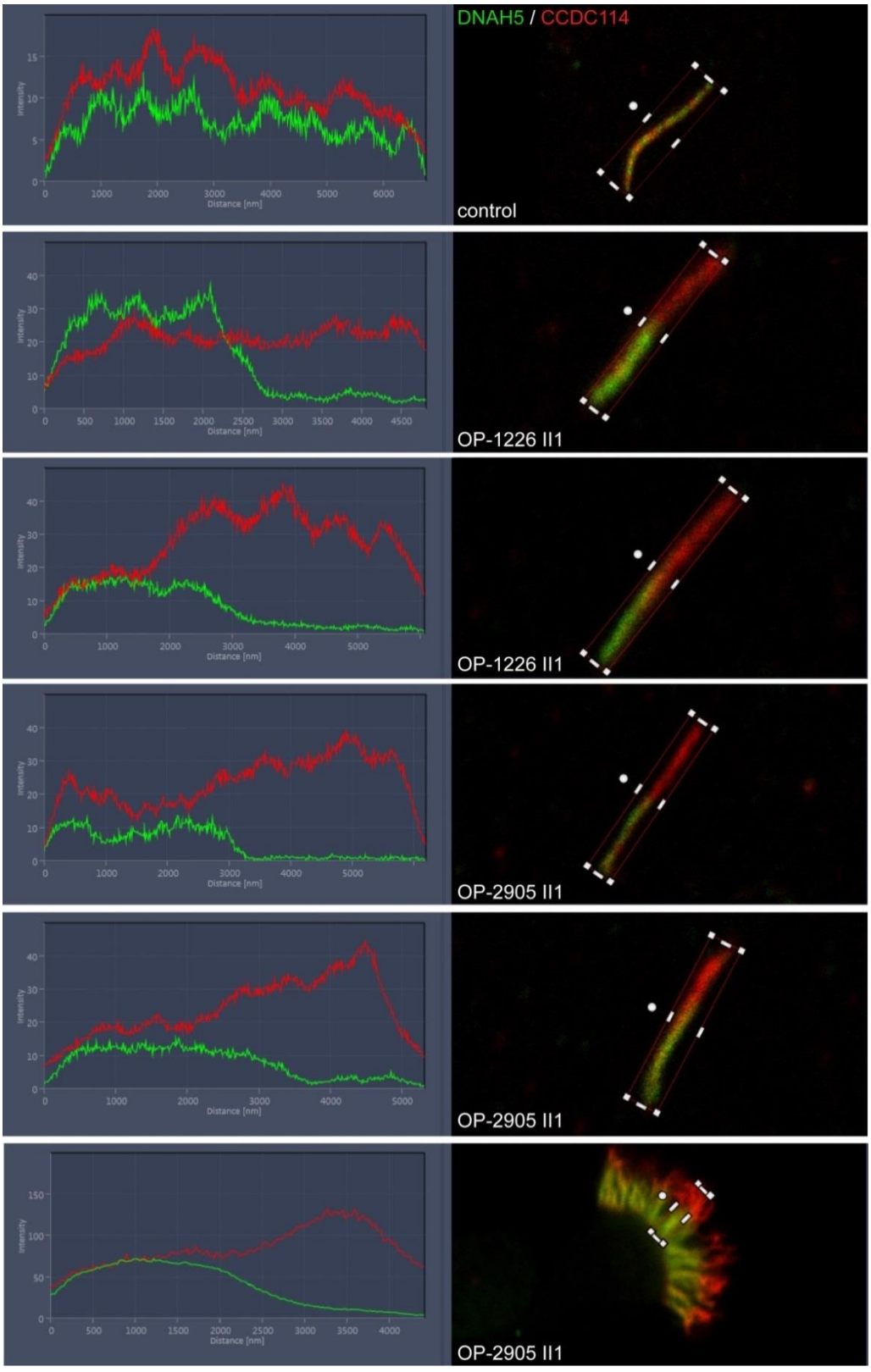

Figure S6. Measurement of the fluorescence intensity along single ciliary axonemes of control and *DNAH9*-mutant respiratory cilia. Intensity profile of DNAH5 signal (green) shows a reduction in the distal part of the ciliary axoneme in *DNAH9*-mutant cilia (OP-1226 II1 and OP-2905 II1) when compared to control cells. In contrast, distribution of CCDC114 (red) is not affected by *DNAH9* mutations. Five representative examples are shown. The red boxes indicate the path of the intensity profile.

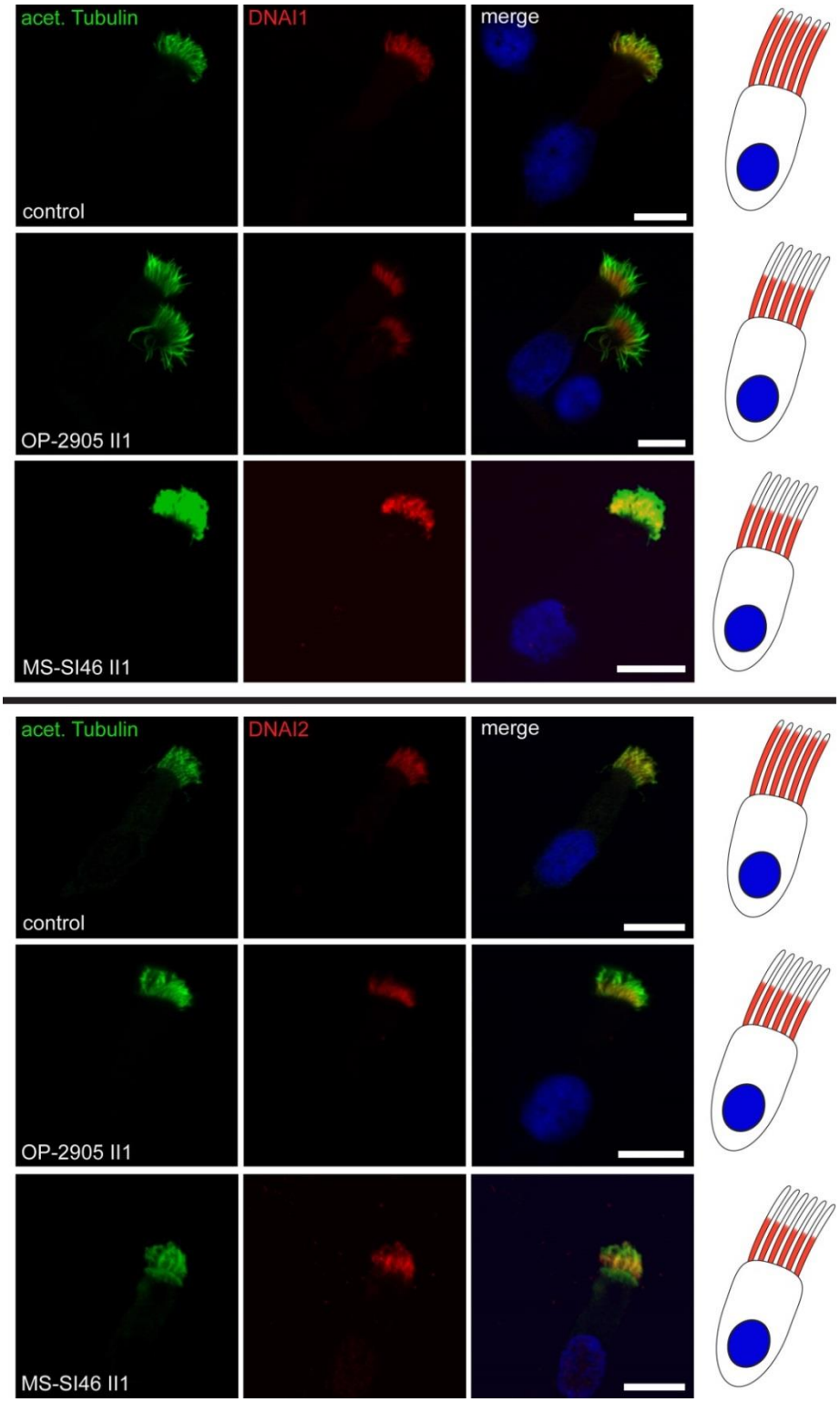

Figure S7. *DNAH9*-mutant cilia lack the distal assembly of the axonemal ODA intermediate dynein chains DNAI1 and DNAI2. Respiratory cilia from controls, individual OP-2905 II1 and individual MS-SI46 II1 were double-labeled with antibodies directed against DNAI1 (red, upper panels) and DNAI2 (red, lower panels) and acetylated tubulin (green). In control cilia, DNAI1 and DNAI2 colocalize with acetylated tubulin (yellow). In contrast, in *DNAH9*-mutant cilia, localization of DNAI1 and DNAI2 was restricted to the proximal part of the ciliary axoneme. Schematic (right side) highlights loss of DNAI1 and DNAI2 (red) in the distal compartment of respiratory cilia. Nuclei were stained with Hoechst33342 (blue). Scale bars represent 10 µm. For each individual, 15 cells were analyzed and stainings were repeated two times.

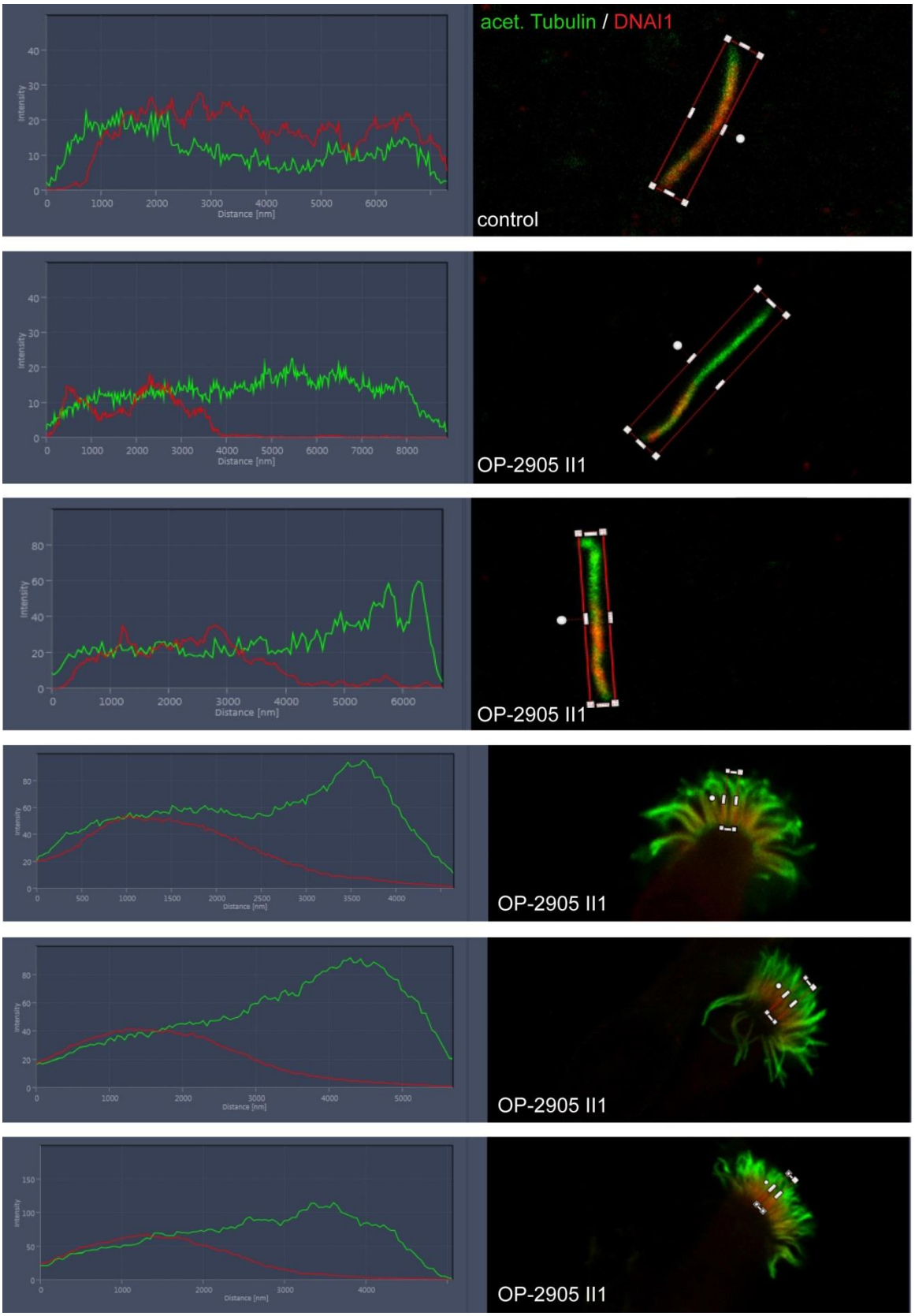

Figure S8. Measurement of the fluorescence intensity along the ciliary axonemes of control and *DNAH9*-mutant respiratory cilia. Intensity profile of DNAI1 signal show a reduction in the distal part of the ciliary axoneme when compared to control cells. Five representative examples are shown. The red boxes indicate the path of the intensity profile.

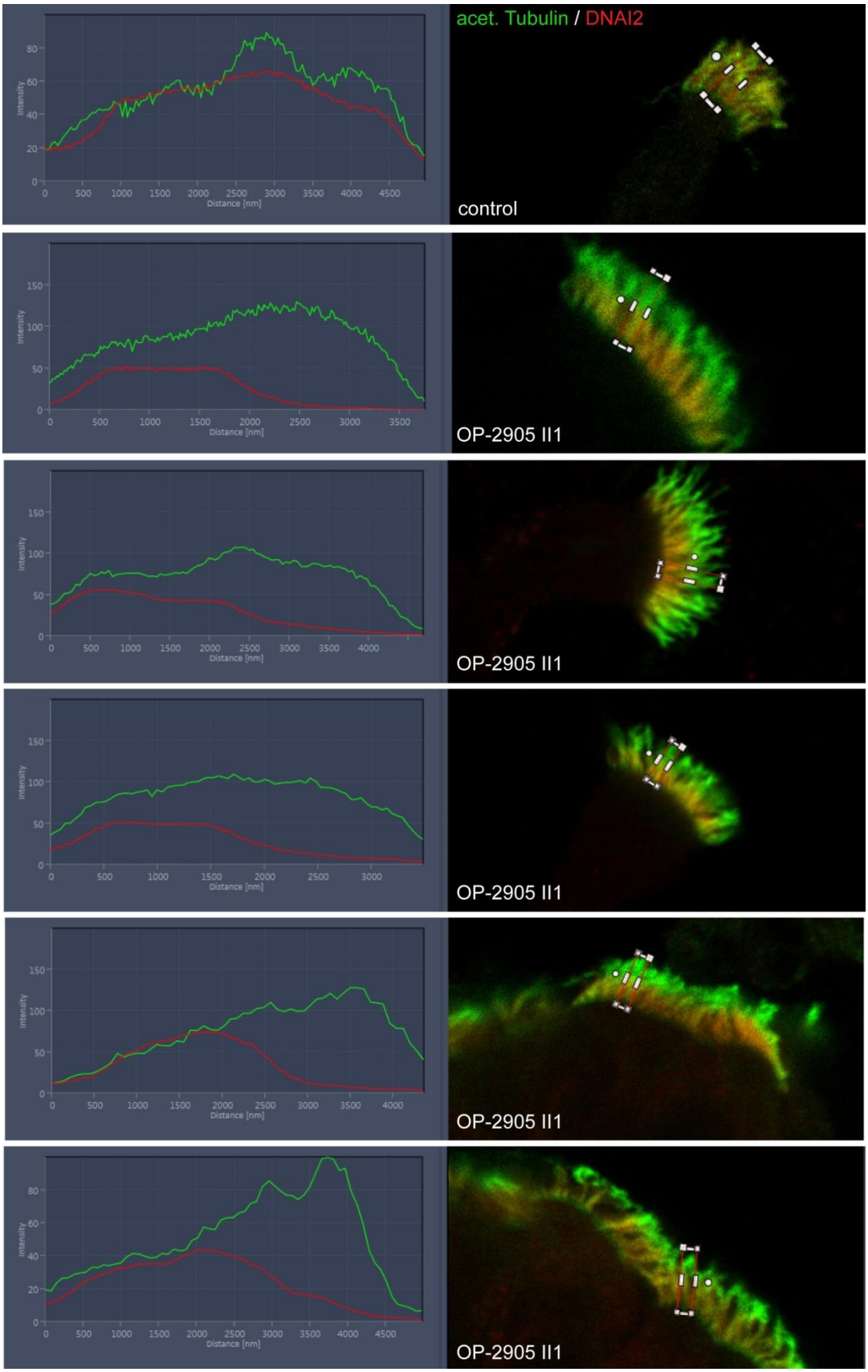

Figure S9. Measurement of the fluorescence intensity along the ciliary axonemes of control and *DNAH9*-mutant respiratory cilia. Intensity profile of DNAI2 signal show a reduction in the distal part of the ciliary axoneme when compared to control cells. Five representative examples are shown. The red boxes indicate the path of the intensity profile.

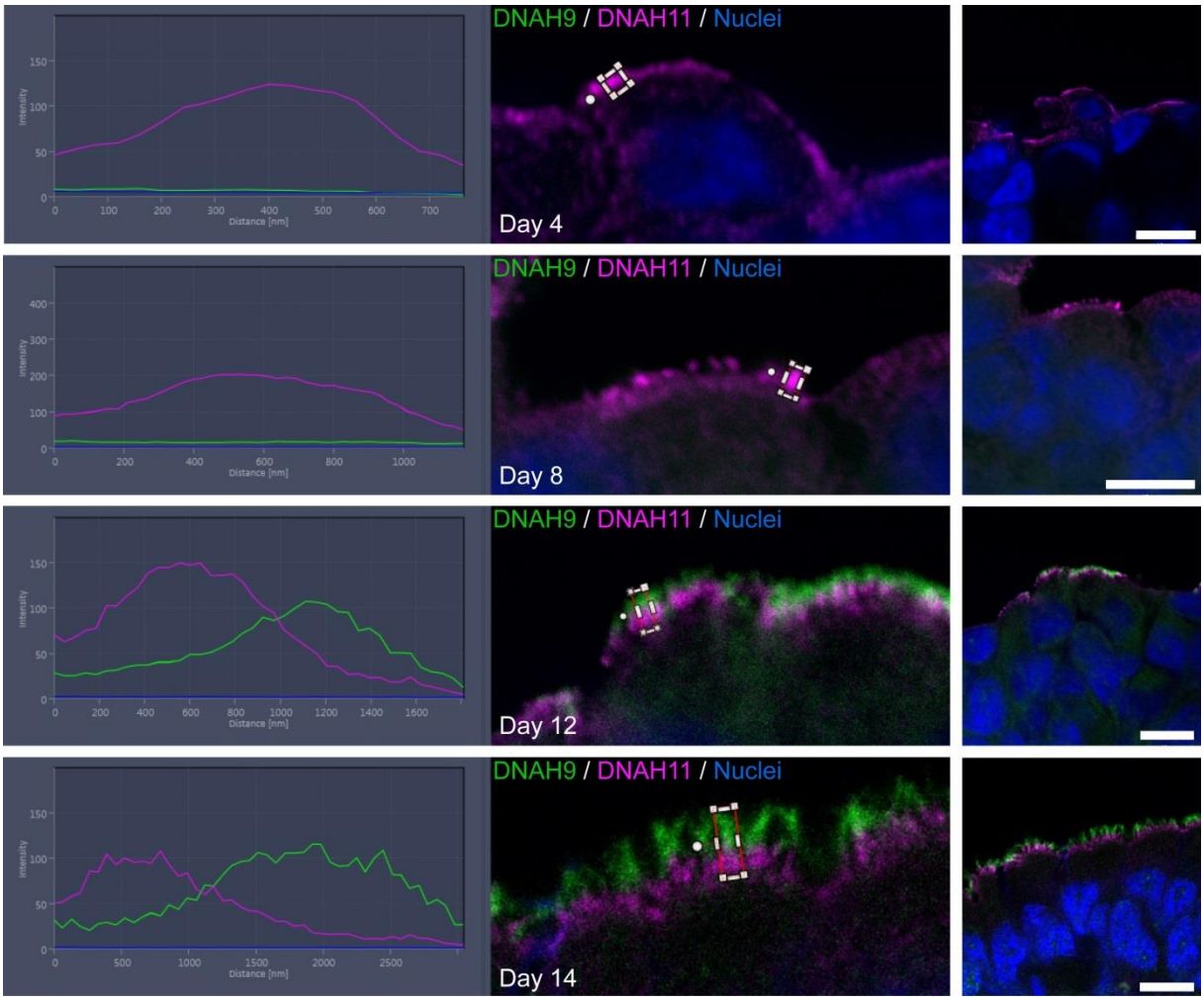

Figure S10. Distribution of the ODA β-HC DNAH9 and DNAH11 in the ciliary axoneme of control cells during ciliogenesis. In early stages of ciliogenesis (day 4-8), only DNAH11 (magenta) is localized to the ciliary axoneme. In later stages of ciliogenesis (day 12-14), DNAH9 (green) is targeted to the distal ciliary axoneme. Nuclei were stained with Hoechst33342 (blue). Scale bars represent 10µm. For each ciliogenesis stage, 5-10 spheroids from 3 different control individuals were analyzed

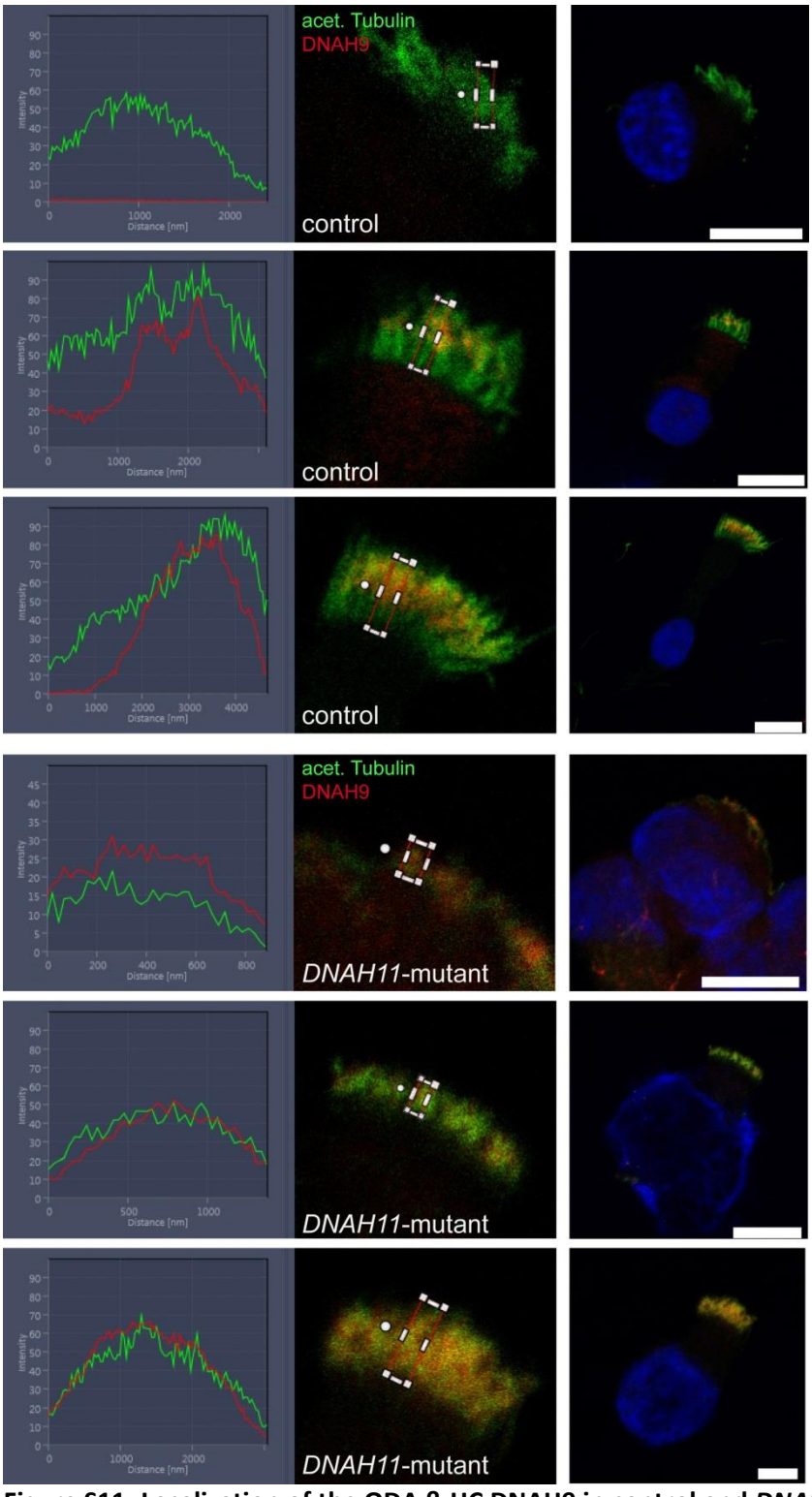

Figure S11. Localization of the ODA β-HC DNAH9 in control and *DNAH11*-mutant cilia with different length. In short cilia DNAH9 (red) is absent from the ciliary axonemes in control cells. In contrast, in *DNAH11*-mutant cells, DNAH9 (red) is already present in short cilia suggesting assembly in early stages of ciliogenesis and is panaxonemal distributed in ciliary axonemes independent of cilia length. Nuclei were stained with Hoechst33342 (blue). Scale bars represent 10µm.

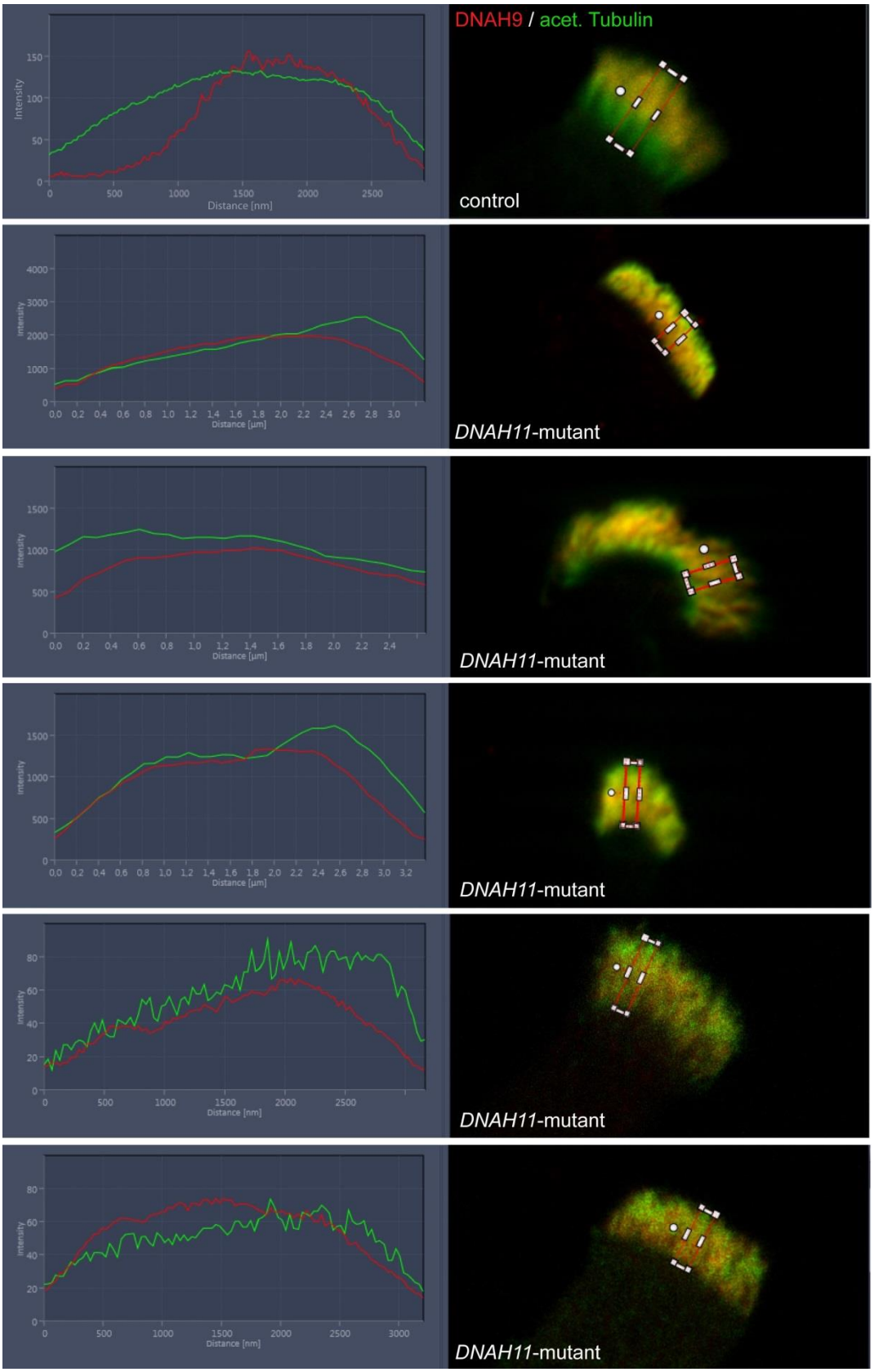

Figure S12. Measurement of the fluorescence intensity along the ciliary axonemes of control and *DNAH11*-mutant respiratory cilia. Intensity profile of DNAH9 (red) show a strong signal in the distal ciliary axoneme in control cells. In contrast, in *DNAH11*-mutants, DNAH9 signal intensity is strong throughout the ciliary axoneme. Five representative examples are shown. The red boxes indicate the path of the intensity profile.

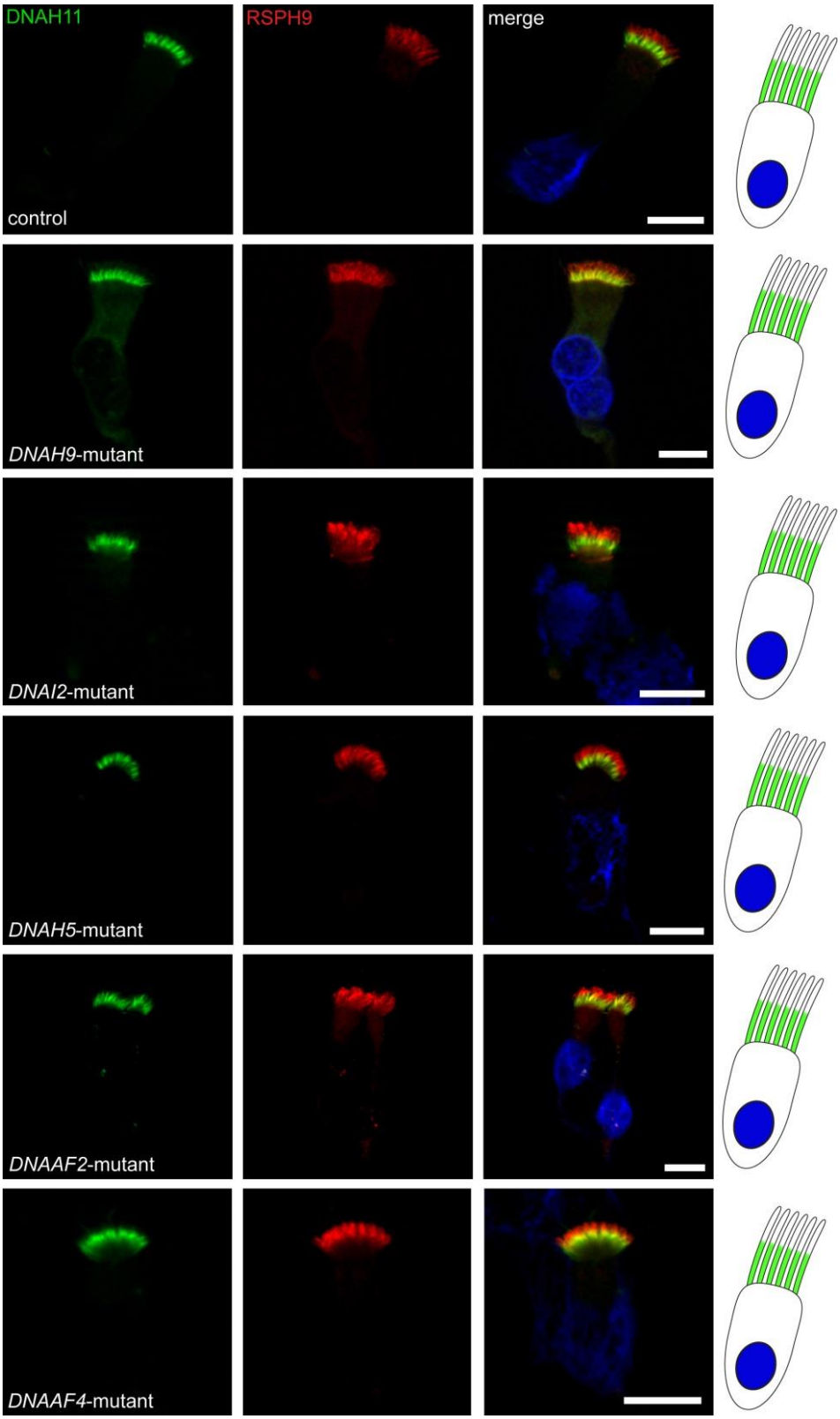

Figure S13. Mutations in *DNAH9, DNAI1, DNAI2, DNAH5*, *DNAAF2 and DNAAF4* do not affect axonemal localization of DNAH11. Respiratory cilia double-labeled with antibodies directed against DNAH11 (green) and RSPH9 (red) show colocalization of DNAH11 with RSPH9 at the proximal part of the cilia in unaffected control cilia and *DNAH9-, DNAI1-, DNAI2-, DNAH5-, DNAAF2- and DNAAF4-*mutant cilia (yellow). Nuclei were stained with Hoechst33342 (blue). Scale bars represent 10 µm. 15 cells were analyzed for each individual.

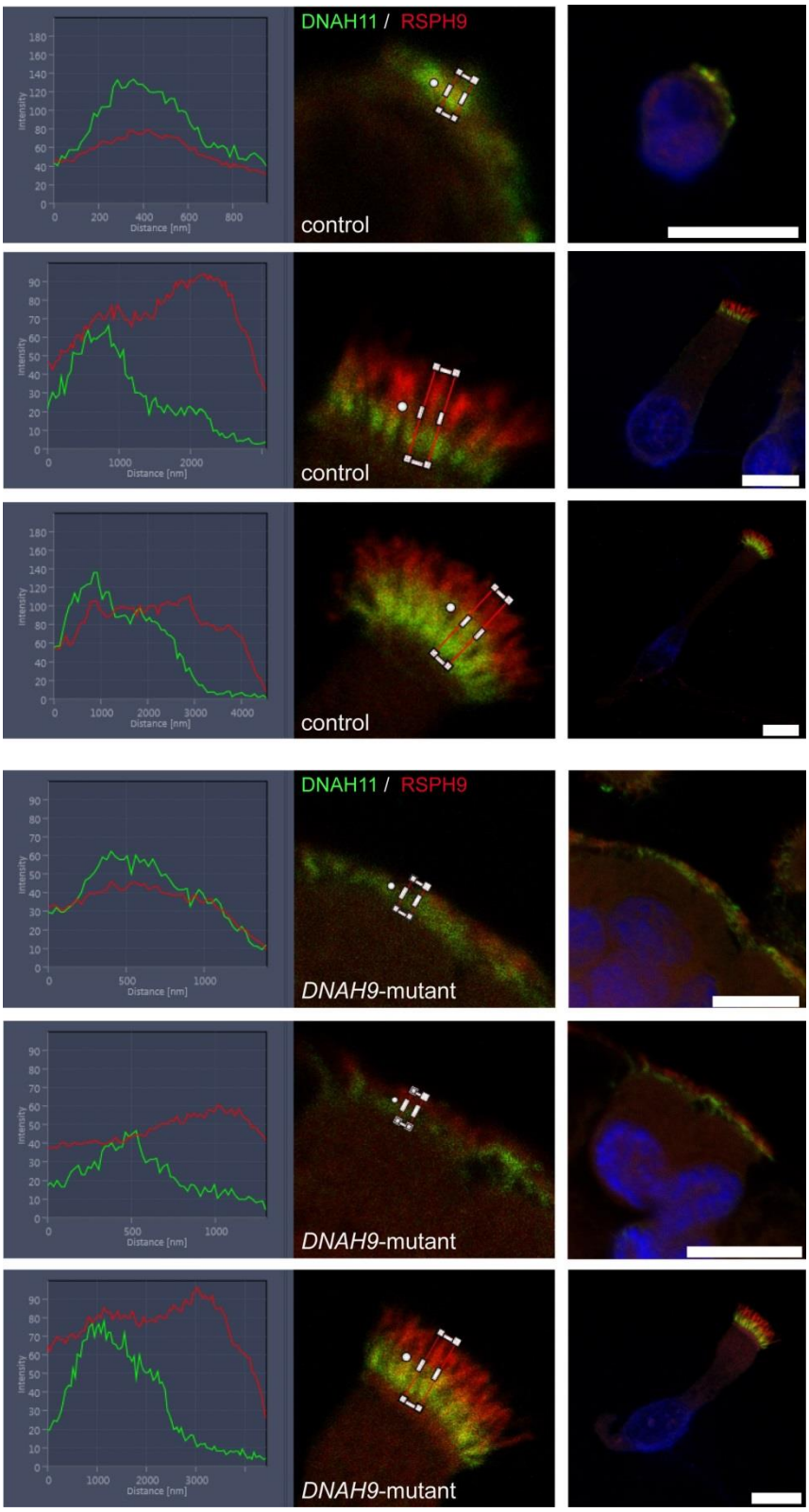

Figure S14. Localization of the ODA β-HC DNAH11 in control and *DNAH9*-mutant cilia with different length. In short cilia, DNAH11 (green) is localized to the ciliary axoneme in control and *DNAH9*-mutant cells indicating axonemal assembly in early stages of ciliogenesis. DNAH11 localization is restricted to the proximal ciliary axoneme in control and *DNAH9*-mutant cilia independent of the cilia length. Nuclei were stained with Hoechst33342 (blue). Scale bars represent 10µm.

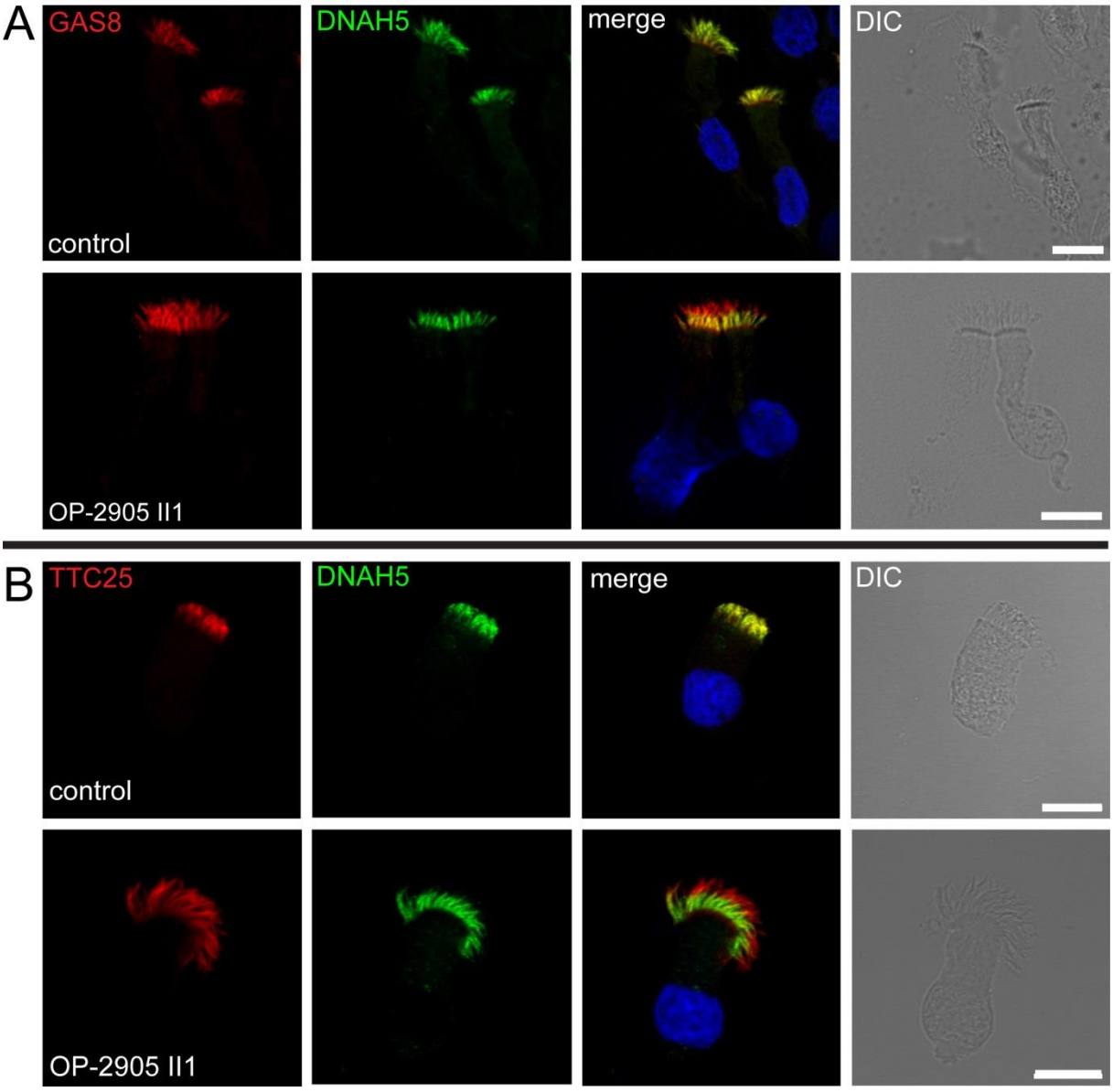

Figure S15. The nexin-dynein regulatory complex (N-DRC) and the outer dynein arm docking complex (ODA-DC) are not affected by loss-of-function mutations in *DNAH9*. Control and *DNAH9*-mutant cilia were co-stained with antibodies directed against N-DRC component GAS8 (A, red) or the ODA-DC component TTC25 (B, red) and an antibody directed against DNAH5 (A and B, green). Localization of GAS8 and TTC25 was not affected by loss of function of *DNAH9.* In contrast, DNAH5 localization is restricted to the proximal part of the ciliary axoneme. Nuclei were stained with Hoechst33342 (blue). Scale bars represent 10 µm. For each individual, 15-20 cells were analyzed and IF-staining with the anti-DNAH5 antibody was repeated two times.

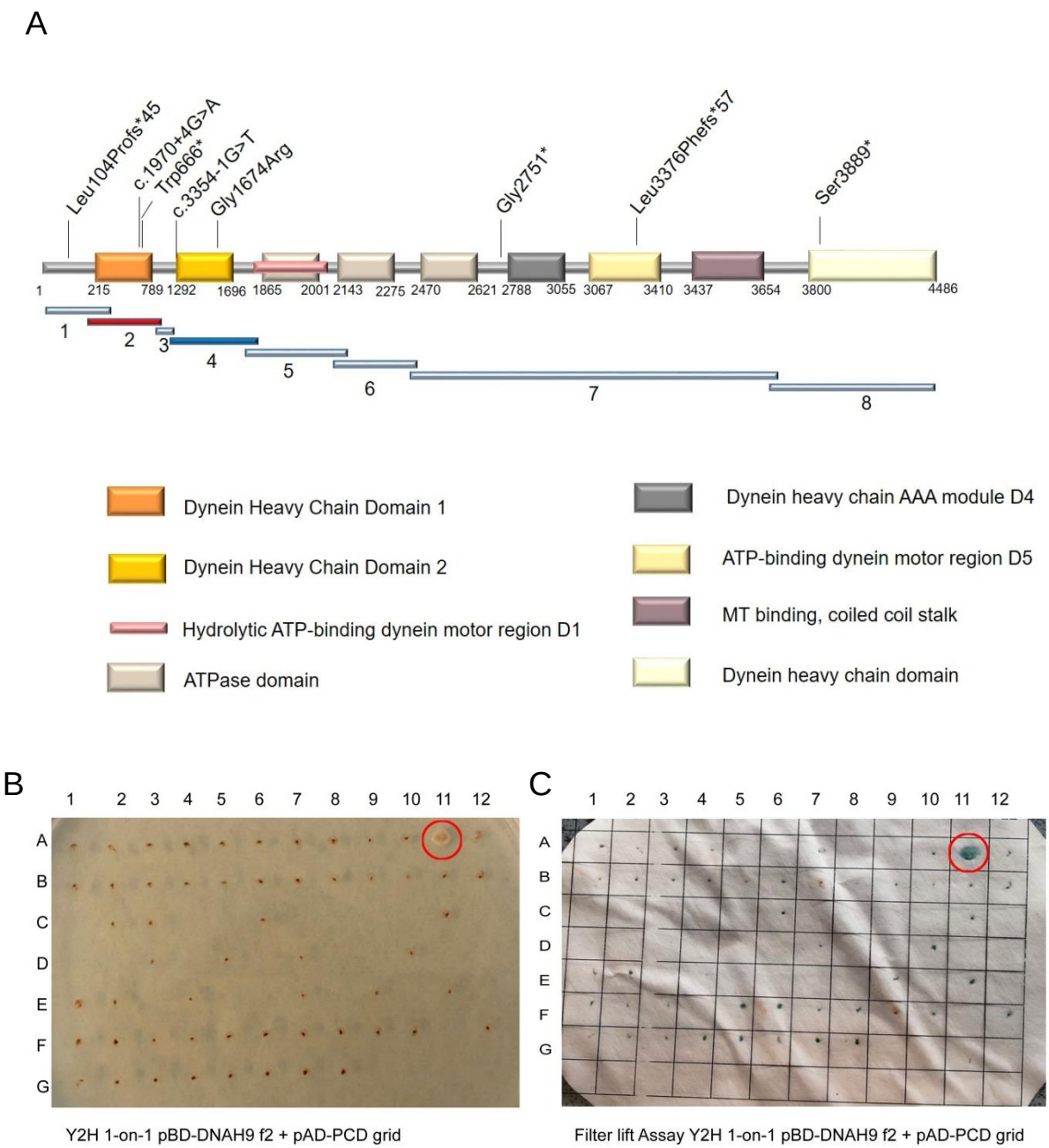

Figure S16. DNAH9 protein-protein interactions tested by Yeast two-hybrid (Y2H) screening. (A) DNAH9 protein schematic with Y2H fragment localization in relation to functional domains. *DNAH9* cDNA was subdivided into 8 fragments due to gene size and subcloned in yeast expression plasmids for Y2H one-on-one screening against a set of known PCD genes and putative interactors (for included proteins and protein-fragments see Table S3-S5). (B) No interaction was observed between pBD-DNAH9-fragment-1 or 3-8 with any protein from the PCD grid (data not shown) while pBD-DNAH9-fragment-2 was found to interact solely with CCDC114 (position A11 marked with a red circle) but not any of the other clones of the PCD grid. Fragment 2 is marked in red in (A). (C) Growth activation at position A11 (pBD-DNAH9f2 + pAD-CCDC114) was confirmed using a filter lift assay where positive clones appear blue.

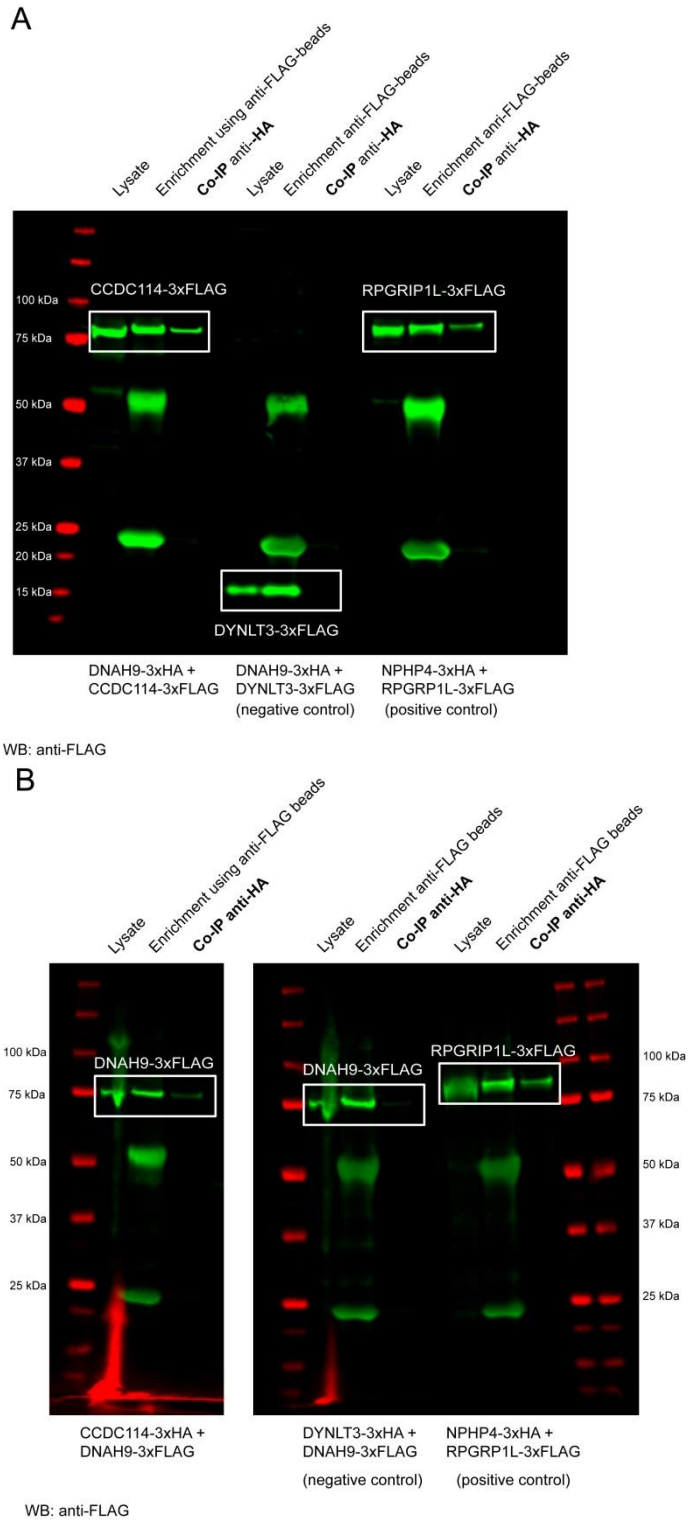

Figure S17. Confirmation of DNAH9 interaction with CCDC114 detected by yeast-two hybrid using co-immunoprecipitation (co-IP). All co-IPs were performed by pulling down HA-tagged protein while enrichment shows pulling down FLAG-tagged protein and membrane staining after western blotting was performed using anti-FLAG antibody. (A) Full gel image of DNAH9-3xHA + CCDC114-3xFLAG co-IP shown in Figure 7, (B) CCDC114-3xHA + DNAH9-3xFLAG co-IP with full gel image shown. Lysate shows the protein content before pulldown, enrichment shows pulled down prey protein. We detected interactions between DNAH9-fragment-2 and CCDC114 full length in both co-IP directions (visible bands in the co-IP lane). Co-IP with NPHP4 and RPGRIP1L was used as a positive control and in the negative control no interaction was detected between DNAH9-fragment-2 and DYNLT3.

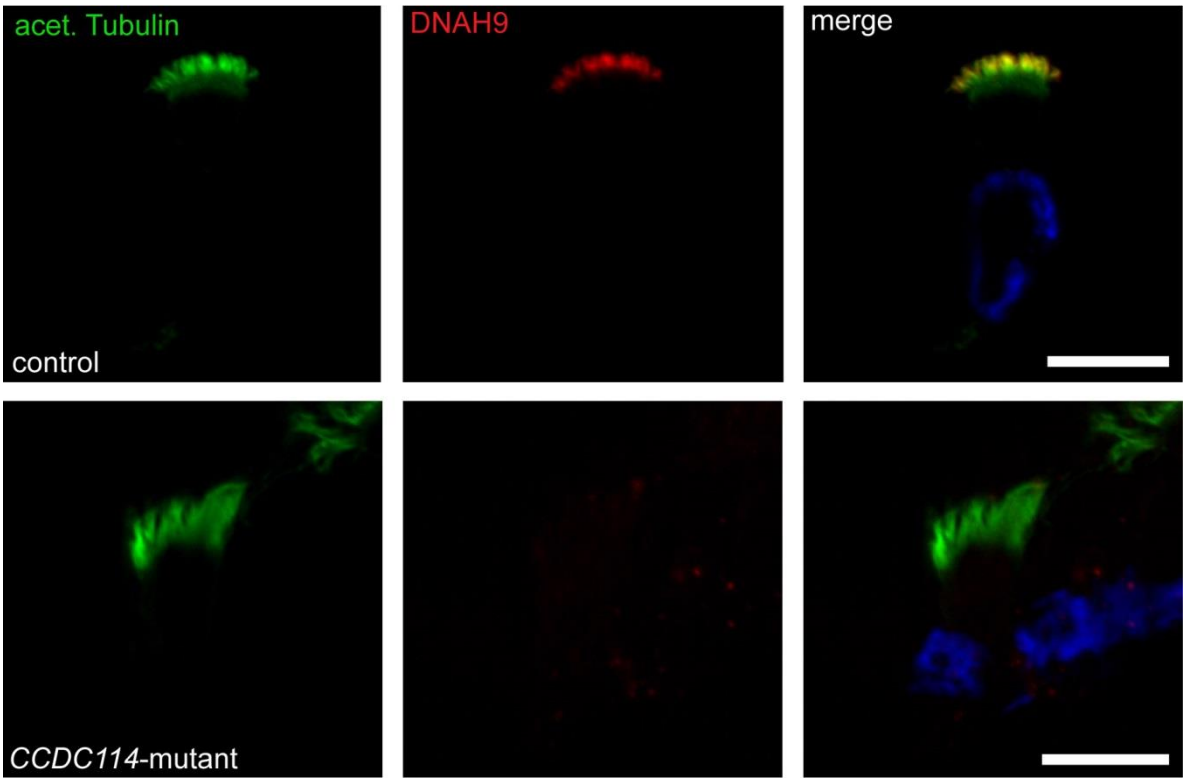

Figure S18. DNAH9 is absent from the ciliary axoneme of *CCDC114*-mutant respiratory cilia. In contrast to healthy controls, DNAH9 (red) is absent or severely reduced in the distal compartment of *CCDC114*-mutant cilia. Ciliary axonemes are counterstained with anti-acetylated tubulin (green). Scale bars represent 10 µm. A total of 15-20 cells were analyzed.

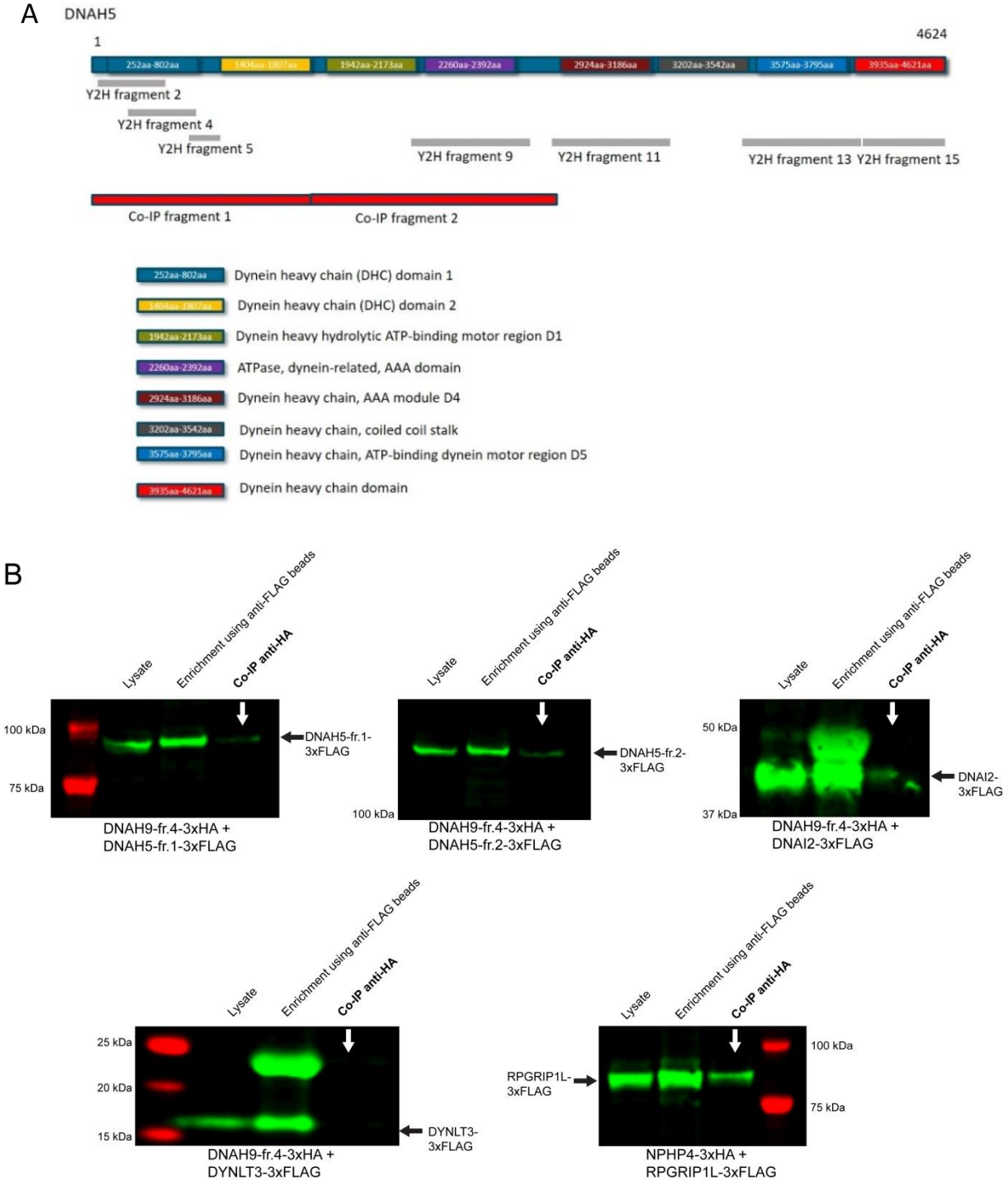
A
DNAH5
1
4624
252aa-802aa
1404aa-1807aa
1942aa-2173aa
2260aa-2392aa
2924aa-3186aa
3202aa-3542aa
3575aa-3795aa
3935aa-4621aa
Y2H fragment 2
Y2H fragment 4
Y2H fragment 5
Y2H fragment 9
Y2H fragment 11
Y2H fragment 13
Y2H fragment 15
Co-IP fragment 1
Co-IP fragment 2
Dynein heavy chain (DHC) domain 1
Dynein heavy chain (DHC) domain 2
Dynein heavy hydrolytic ATP-binding motor region D1
ATPase, dynein-related, AAA domain
Dynein heavy chain, AAA module D4
Dynein heavy chain, coiled coil stalk
Dynein heavy chain, ATP-binding dynein motor region D5
Dynein heavy chain domain
B
Lysate
Enrichment using anti-FLAG beads
Co-IP anti-HA
100 kDa
75 kDa
DNAH5-fr.1-3xFLAG
DNAH9-fr.4-3xHA +
DNAH5-fr.1-3xFLAG
100 kDa
DNAH5-fr.2-3xFLAG
DNAH9-fr.4-3xHA +
DNAH5-fr.2-3xFLAG
50 kDa
37 kDa
DNAI2-3xFLAG
DNAH9-fr.4-3xHA +
DNAI2-3xFLAG
25 kDa
20 kDa
15 kDa
DYNLT3-3xFLAG
DNAH9-fr.4-3xHA +
DYNLT3-3xFLAG
RPGRIP1L-3xFLAG
100 kDa
75 kDa
NPHP4-3xHA +
RPGRIP1L-3xFLAG
WB: anti-FLAG

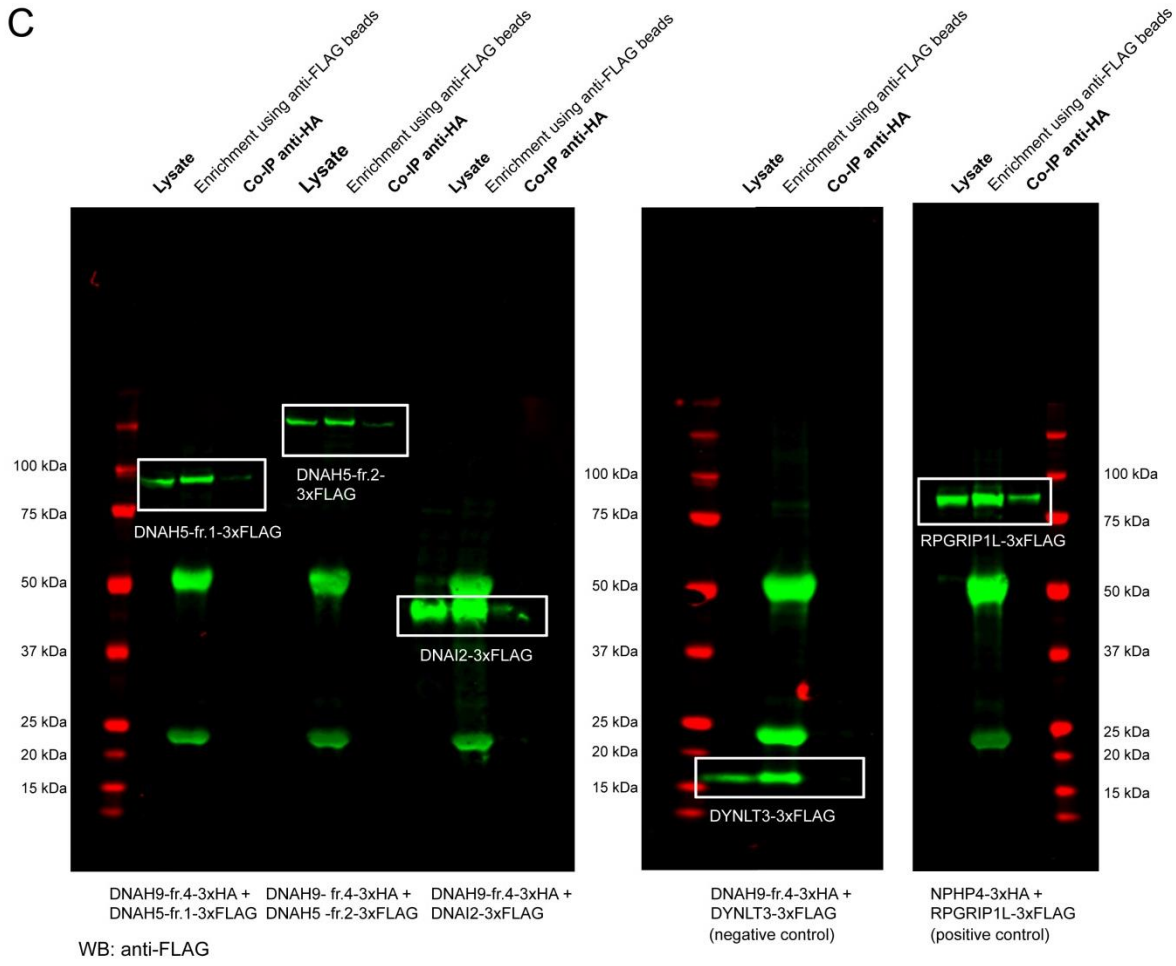

Figure S19. DNAH9 protein-protein interactions with outer dynein arm subunits tested by co-immunoprecipitation (co-IP). (A) DNAH5 protein schematic with functional domains marked as well as localization of DNAH5-co-IP-fragment-1 and -2. No interaction between any of the DNAH5-Y2H-fragments indicated in the schematic and any of the eight DNAH9-fragments (shown in figure S15) was detected. (B) We therefore proceeded to test larger DNAH5-fragments conserving functional domain integrity by co-IP and focused on DHC domains as we previously found DHC1 to interact with CCDC114 full length (Figure S15). This revealed interaction between DNAH9-fragment-4 containing DHC2 and DNAH5-fragment-1 and -2 as well as full length DNAI2. Lysate shows protein content before pull down, enrichment shows pulled down prey protein. co-IP shows prey protein pulled down by the bait protein, showing protein-protein interaction between prey and bait proteins. NPHP4 interacted with RPGRIP1L (positive control) while no interaction was detected between DNAH9-fragment-4 and DYNLT3 (negative control). (C) Full gel image shown.

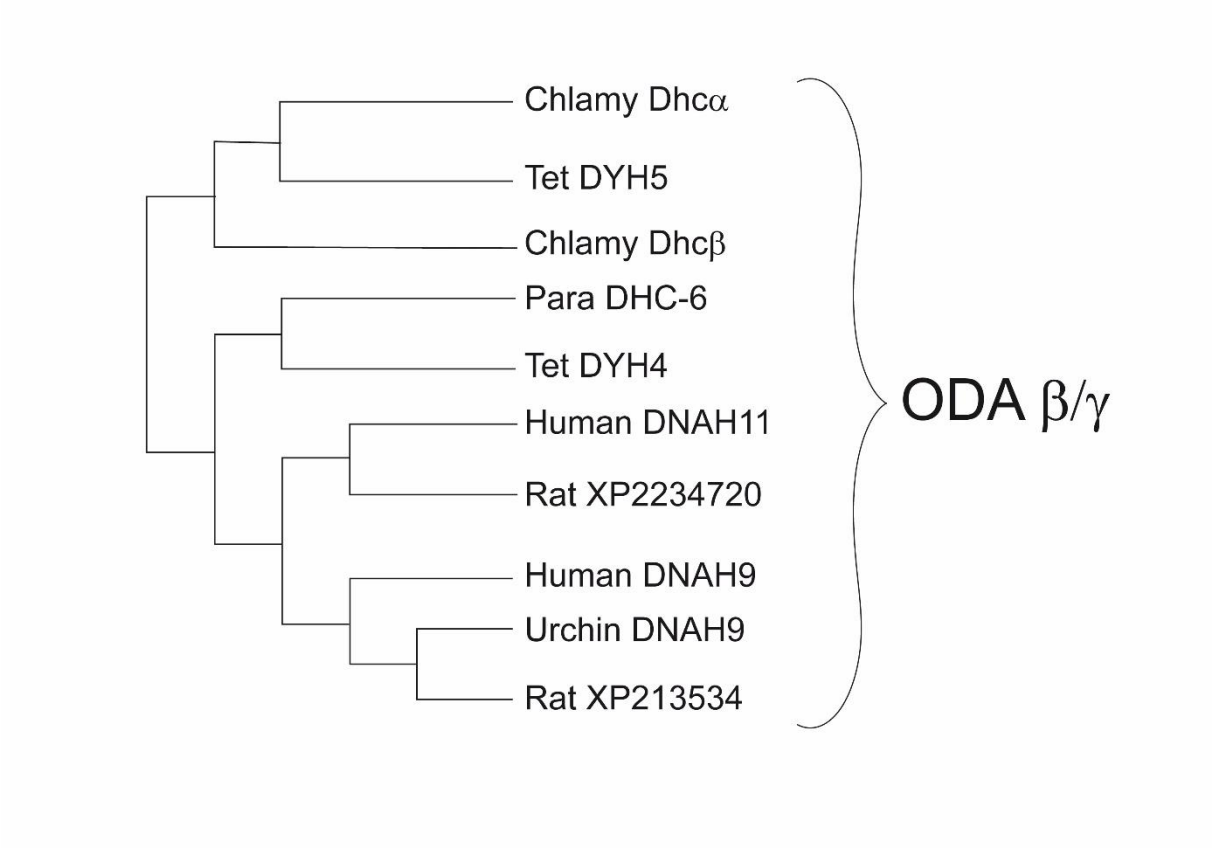

Figure S20. Evolution of the *Chlamydomonas* ODA β-heavy chain human orthologs DNAH9 and DNAH11. Reconciled gene tree of axonemal dynein heavy chain genes in *Homo sapiens* (Human), *Rattus norvegicus* (Rat), *Chlamydomonas reinhardtii* (Chlamy), *Tetrahymena sp.* (Tet), *Paramecium sp.* (Para), *Strongylocentrotus purpuratus* (Urchin). In the green alga *Chlamydomonas reinhardtii* three distinct outer dynein arm heavy chains (ODA HC) have been identified: α-HC, β-HC and γ-HC. In contrast, in humans, there are two orthologues of the β-HC. DHC/DYH: Dynein heavy chain, ODA: outer dynein arm.

Table S1. Overview of the diagnostic PCD-gene panel. Genes included in the gene panel related to ciliary motility, PCD and laterality defects.

Gene	Locus	References
DNAH9	**17p12**	**not published**
DNAH5	**5p15**	**Olbrich et al., 2002**
DNAH11	**7p15.3**	**Bartoloni et al. 2002; Schwabe et al., 2008**
DNAI1	**9p13.3**	**Pennarum et al., 1999; Zariwala et al., 2006**
DNAI2	**17q25.1**	**Loges et al., 2008**
TXNDC3/NME8	**7p14.1**	**Duriez et al., 2007**
DNAL1	**14q24.3**	**Mazor et al., 2011**
CCDC103	**17q12**	**Panizzi et al., 2012**
CCDC114	**19q13.33**	**Onoufriadis et al., 2013; Knowles et al., 2013**
ARMC4	**10p21**	**Hjeij et al., 2013**
CCDC151	**19p13.2**	**Hjeij et al., 2014**
TTC25	**17q21.2**	**Wallmeier et al., 2016**
LRRC50/DNAAF1	**16q24**	**Loges et al., 2009; Duquesnoy et al., 2009**
KTU/DNAAF2	**14q21.3**	**Omran et al., 2008**
DNAAF3	**19q13**	**Mitchison et al., 2012**
DYX1C1/DNAAF4	**15q21**	**Tarkar et al., 2013**
SPAG1	**8q22**	**Knowles et al., 2013**
ZMYND10	**3p21.3**	**Moore et al., 2013; Zariwala et al.,2013**
HEATR2/DNAAF5	**7p22.3**	**Horani et al., 2012**
C21ORF59	**21q22.1**	**Austin-Tse et al., 2013**
LRRC6	**8q24**	**Kott et al., 2012; Horani et al., 2013**
PIH1D3	**Xq22.3**	**Paff et al., 2017; Olcese et al., 2017**
RPGR	**Xp21.1**	**Moore et al., 2006**
OFD1	**Xp22**	**Budny et al., 2006**
HYDIN	**16q22**	**Olbrich et al., 2012**
STK36	**2q35**	**Edelbusch et al., 2017**
RSPH1	**21q22.3**	**Kott et al., 2013; Knowles et al., 2014**
RSPH9	**6p21**	**Castleman et al., 2009**
RSPH4A	**6q22**	**Castleman et al., 2009**
RSPH3	**6q25.3**	**Jeanson et al., 2015**
CCDC164	**2p23**	**Wirshell et al, 2013**
CCDC65	**12q13.12**	**Austin-Tse et al, 2013; Horani et al, 2013**
GAS8	**16q24.3**	**Olbrich et al, 2015**
CCDC39	**3q26**	**Merveille et al, 2011**
CCDC40	**17q25**	**Becker-Heck et al, 2011**
CCNO	**5q11.2**	**Wallmeier et al., 2014**
MCIDAS	**5q11.2**	**Boon et al., 2014**
CCDC11	**18q21.1**	**Narasimhan et al., 2015**
ENKUR	**10p12.1**	**Sigg et al., 2017**

Table S2. Exome Filtering details for MS-SI46 II1. A total number of 314,219 variants were filtered.

Total number of variants	**314,219**
Total non-synonymous, stop, frameshift, in-frame indels and splicing variants	**14,287**
Of which < 1% MAF [1]	**1144**
Missense non-synonymous variants < 1% MAF[1]	**821**
Splicing variants < 1% MAF[1]	**125**
Frameshift variants < 1% MAF	**64**
In-frame insertions and deletions < 1% MAF[1]	**58**
Stop Gain < 1% MAF[1]	**30**
Stop Loss < 1% MAF[1]	**6**
Unknown Function[1]	**40**
Homozygous non-synonymous missense variants < 1% MAF[2] *ARHGEF5*: rs752820457 : NM_005435:c.G1504T:p.Val502Leu *C12orf63:* NM_001306084: c.G5164A:p.Gly1722Ser (novel variant) *DMBT1*: rs186303194: NM_017579: c.G1873A:p.Asp625Asn *IMMT*: rs368769430: NM_001100169: c.G340A:p.Val114Ile *TSSC4:* rs746739443: NM_001297659: c.C370T:p.Arg124Trp	**5**
Homozygous splicing variants < 1% MAF[2] *NPIPB3:* rs767458164 (non-canonical splice position)	**1**
Homozygous frameshift variants < 1% MAF[2] *ATXN3*[#]*:* NM_001164782: c.67_68insCAGCAGCAGCAGCAGCA:p.Leu23Serfs*30, novel variant *DNAH9:* NM_001372:c.10126dupT, p.Leu3376Phefs*57 (novel varaint)	**2**
Homozygous in-frame insertions and deletions < 1% MAF[2]	**-**
Homozygous stop gain < 1% MAF[2]	**-**
Homozygous stop loss < 1% MAF[2] *CYB5D1:* rs201717097: NM_144607: c.T685C:p.X229Gln	**1**
Homozygous Unknown Function[2]	**-**

[1] MAF < 1% in ExAc, 1000 genomes, dbSNP

[2] MAF < 1% in ExAc, 1000 genomes, dbSNP, gnomAD exomes, gnomAD genomes, TOPMED, Clinseq-Agilent project

[#] allele frequency > 1% in in-house exomes

Novel variant: Variant not previously reported in population databases named under [2]

Table S3. Overview of proteins screened by Yeast two hybrid (Y2H) one-on-one for interaction with DNAH9-fragments (PCD grid). A total of 31 proteins were screened for interaction with DNAH9.

Outer dynein arm components	DNAI1
	DNAI2
	TXNDC3
	DNAH11 (partial)
	DNAH5-fragment-1
	DNAH5-fragment-4
	DNAH5-fragment-5
	DNAH5-fragment-9
	DNAH5-fragment-11
	DNAH5-fragment-13
	DNAH5-fragment-16
Outer dynein arm docking complex	CCDC151
	CCDC114
	TTC25
	ARMC4
Dynein axonemal assembly factors	DNAAF1
	DNAAF2
	DNAAF3
	DNAAF4
	PIH1D3
	SPAG1
	LRRC6
	ZMYND10
	C21ORF59
	CCDC103
Inner dynein arm components	DNAH7-fragment-1
	DNAH7-fragment-2
	DNAH7-fragment-4
	DNAH7-fragment-7
	DNAH7-fragment-9
	DNAH7-fragment-11
Interflagellar transport	IFT46
	WDR69
Chaperones	HSP70-fragment-1
	HSP70-fragment-2
	HSP70-fragment-3
	HSP90-fragment-1
	HSP70-fragment-2
Others	KIFC1-fragment-1
	KIFC1-fragment-2
	DYNLT1
	DYNLT3
	DYNLRB1
	DYNLRB2
	DYNLL1
	DCTN1

Table S4. DNAH9-fragment interactions detected by Yeast two-hybrid (Y2H). DNAH9-fragment-2 interacts with the CCDC114.

DNAH9 Y2H Fragment	DNAH9 amino acids	Y2H one-on-one pBD-DNAH9 + pAD-PCD grid interactions
DNAH9-fragment-1	1-300	-
DNAH9-fragment-2	201-859	CCDC114 full length
DNAH9-fragment-3	800-1250	-
DNAH9-fragment-4	1200-1800	-
DNAH9-fragment-5	1750-2150	-
DNAH9-fragment-6	1999-2399	-
DNAH9-fragment-7	2299-3749	-
DNAH9-fragment-8	3689-4486	-

Table S5. DNAH5-fragments used for DNAH9 Yeast-two Hybrid (Y2H). A total of 7 fragments were generated for testing in Y2H.

DNAH5 Y2H Fragment	DNAH5 amino acids
DNAH5-fragment-2	235-635
DNAH5-fragment-4	420-820
DNAH5-fragment-5	800-1200
DNAH5-fragment-9	2100-2500
DNAH5-fragment-11	2800-3200
DNAH5-fragment-13	3500-3900
DNAH5-fragment-16	4250-2621

Table S6. DNAH5-fragments used for co-immuno precipitation (Co-IP) with DNAH9 fragment 2. Two DNAH5-fragments were used for Co-IP.

DNAH5 Fragment	DNAH5 amino acids
DNAH5-fragment-1	1-1807
DNAH5-fragment-2	1807-2924

Supplemental Methods

Mutational Analyses

For OP-2905 II1, Next Generation Sequencing (NGS) was performed using a diagnostic PCD-gene panel for 39 genes previously associated with PCD and/or laterality defects (Table S1) (Agilent Technologies, custom made panel). DNA samples were enriched with SureSelect™ Target Enrichment Kit (Agilent Technologies, Santa Clara, USA). Libraries were sequenced on a MiSeq or a NextSeq 500 platform (Illumina, San Diego, USA) using 2× 150 bp paired-end sequencing. A triple bioinformatics pipeline was set up to secure detection of SNVs and Indels. The first pipeline included the CASAVA suite v1.8.2 from Illumina for demultiplexing, generation of fastq files, mapping of the reads and variant calling. In the second pipeline, reads mapping was performed using Burrow-Wheeler Aligner, recalibration and variant calling were performed using Picard and GATK software; data were imported into a homemade bioinformatics pipeline which mainly based on wANNOVAR backbone[1]. The third pipeline represents the GensearchNGS software tool (PhenoSystems SA). Variants detected by these pipelines were then annotated by Alamut Batch (Interactive BioSoftware, Rouen, France). For each sequencing run, quality reports integrating the number of clusters/mm2 , percentage of bases with a Qscore >30, FastQC reports, percentage of mapped reads, on- and off-targets percentages, percentage of covered bases and mean sequencing depth were generated. Detected variants were confirmed on the original blood sample by PCR-amplification of genomic fragments and Sanger sequencing. Our captured design and NGS workflow ensured coverage of more than 99% of targeted bases and a read depth of 50× at all positions. Only at few positions read depth was smaller and those positions were controlled by Sanger sequencing. Pathogenicity was established according to the American College of Medical Genetics[2].

For WES (MS-SI46 II1), Exomic sequences from DNA samples were enriched with SureSelect Human All Exon V.6 Kit (Agilent Technologies, Santa Clara, California, USA) according to the manufacturerer protocol followed by sequencing on a Hiseq PE150 (Illumina, San Diego, California, USA). Read alignment and variant calling were performed based on Burrows-Wheeler (BWA)/GATK-pipeline using default parameters with the human genome assembly hg19 (GRCh37) as reference.

Variant were stored and annotated using vtools and ANNOVAR softwares. Following alignment and variant calling, serial variant filtering was performed for variants with a MAF equal or less than 1% in ExAc, 1000 genome project and esp6500 databases, coding variants or variants within 5 bp of exon-intron boundaries, and genes carrying bi-allelic variants with prioritization of homozygous variants in consanguineous pedigrees and genes carrying two different heterozygous variants in non-consanguineous pedigrees. Remaining homozygous variant were additionally manually filtered for MAF< 1% in Genome Aggregation Database (gnomad.broadinstitute.com), TOPMED (Transition for Precision Medicine program (https://www.nhlbi.nih.gov/science/trans-omics-precision-medicine-topmed-program)) and Clinseq-Agilent project (https://www.genome.gov/20519355/clinseq-a-largescale-medical-sequencing-clinical-research-pilot-study/) databases with frequencies retrieved from ensembl. Obligate loss-of-function variants such as canonical splice variants, frameshift and stop mutations were prioritized over missense variants, but missense variants were not excluded from the analysis. BAM files were visually inspected for homozygous CNVs in all genes known to cause PCD or laterality defects. All the variants passing these filters were subsequently inspected at aligned read level with the aim of avoiding false call due to misalignment or low-depth of coverage. Variants left after filtering are shown in Table S2. *DNAH9* variants were prioritised due to the fact *DNAH9* encodes an ODA component and laterality defects have been previously found to result form mutations in other ODA genes.

For individual AM II.1, target capture using Illumina Trusight One targeting 12 Mb was performed followed by sequencing on a Illumina HiSeq 2500 machine and targeted analysis performed for genes previously associated with heterotaxy in human and mice as well as known cilia motiliy apparatus components. In addition to the filtering described above, variants were further filtered using an in-house background population variant frequency estimated based on compilation of 2000 Slovenian exomes.

For individual MD II.1, a clinical diagnostic exome, using the Agilent SureSelect XT Clinical Research Exome kit was performed and sequenced on the Illumina HiSeq 2500 with 100bp paired-end reads filtered as described above.

RNA-Seq

In previous studies, we already generated human transcriptome profiles by Next Generation Sequencing using the Ion Proton™ and mRNA isolated from respiratory cells grown on air liquid interface (ALI)-culture to full differentiation, nasal brushing biopsies and EBV-transduced lymphocytes, each obtained from healthy controls[3]. In addition, we previously analyzed transcript variants using the SureSelect™ RNA Target Enrichment Kit (Agilent Technologies) for RNA-seq in combination with our custom-designed 39 PCD-associated gene panel (Agilent Technologies, Table S1) and the NextSeq 500 Illumina® platform. Routine RNA-seq workflow consisted of quality control and preprocessing of raw data, read alignment, transcriptome reconstruction, expression quantification, and differential expression analysis. Transcriptome data were aligned using both unspliced (e.g. Burrow-Wheeler Aligner, Bowtie) and spliced aligner (e.g. TopHat, GSNAP). Further analysis of transcriptome data included differential expression analysis (e.g. Cufflinks, MISO, IDEG6), alternative splicing events (e.g. TopHat, Splicing-Compass), variant detection (GATK), pathway analysis (e.g. GSAA SeqSP, GSEA) and co-expression network (e.g. GSCA, WGCNA).

Yeast two Hybrid (Y2H) one-on-one screening:

We performed a Y2H screen using DNAH9 as a bait to test interaction with several proteins previously associated with PCD: known ODA components (such as DNAH5-fragments, DNAI1 and DNAI2), ODA docking complex proteins, dynein axonemal assembly factors, inner dynein arm components, intraflagellar transport proteins, chaperones and other proteins (Table S3, S4 and S5). Direct interaction between DNAH9 and possible interactors was tested as previously described [4]. In brief, Human *DNAH9, DNAH7* and *DNAH5* cDNAs were purchased from Origene, *DYNLT3* and *DYNLRB1* cDNAs purchased from genscript. Clones for *DYNLT1*, *DYNLL1*, *DYNLRB1* and *DCTN1* have been previously described[5]. All other cDNAs have been previously cloned by nested PCR (for PCD genes, from human bronchial epithelial cell cDNA (ScienCell) using KOD polymerase according to manufacturer's directions as previously described.[4] Due to their large size (making it unsuitable for

Y2H screening), *DNAH9*, *DNAH7* and *DNAH5* cDNAs were subcloned in fractions and similarly to all other cDNAs, recombined with pDONR201 Gateway vector via BP Clonase II reaction. cDNAs were then subcloned into 3xHA- and 3xFLAG-epitope-tagged Gateway destination vectors via LR Clonase reaction, according to the manufacturers instuctions (Gateway cloning technology (Thermo Fisher Scientific). All cDNA clones were confirmed by sequence analysis and matched RefSeq gene accession numbers. We then performed one-on-one testing of all eight DNAH9-fragments (see Figure 1 and Figure S15 for fragment location within the protein) against the grid of PCD proteins (see Table S3 for grid composition) in both directions (pAD-DNAH9 + pBD-PCD-grid and pBD-DNAH9 + pAD-PCD grid) as previously described, using a GAL4 based system[4]. Interactions were analysed by assessment of reporter gene activation based on growth on selective media. This revealed only one interaction of DNAH9-fragment-2 with full length CCDC114 which was confirmed using a β-galactosidase colorimetric filter lift assays (*LacZ* reporter gene).

Co-Immunoprecipitation

Human embryonic kidney (HEK293T) cells (European Collection of Cell Cultures) were cultured under standard conditions at 37 °C and 5% CO_2 in DMEM-F12 Glutamax medium (Life Technologies) with 10% fetal bovine serum (Life Technologies). Proteins tagged with 3xHA- and 3xFLAG-epitopes were generated from Gateway entry clones by LR Clonase reaction. All clones were confirmed by sequence analysis to match appropriate RefSeq genes. Overexpression of tagged versions of the proteins in HEK293T cells, whole-cell extracts and Western blots were conducted as previously described[4]. Plasmids expressing 3xHA-tagged DNAH9-fragment-2 were co-transfected with plasmids either expressing 3xFLAG-tagged CCDC114 or DNAH5-fragments or vice versa, 3xFLAG-tagged DNAH9-fragment-2 was co-transfected with 3xHA-tagged CCDC114 or DNAH5-fragments. 48 hours after transfection, cells were lysed on ice using lysis buffer (50 mM Tris-HCl [pH 7.5], 150 mM NaCl, 1% NP-40) supplemented with complete protease inhibitor cocktail (Roche). Lysates were incubated with anti-HA affinity matrix (Roche) for 2–3 hours at 4°C. After incubation, beads with bound protein complexes were washed in ice-cold lysis buffer. Subsequently, 4X NuPAGE sample

buffer was added to the beads and heated for 10 min at 70°C. Beads were pelleted by centrifugation, and supernatant was analyzed on NuPAGE Novex 4%–12% Bis-Tris SDS-PAGE gels. After blotting overnight at 4°C, blots were incubated with mouse anti-FLAG. Fluorescence signal was analyzed on a LI-COR Odyssey 2.1 infrared scanner.

Primary respiratory cell cultures and ciliogenesis

Respiratory epithelial cells from nasal brushings or polyps were obtained from healths controls or individuals (no PCD individuals) that underwent ear, nose, and throat (ENT) surgery. The removed tissue was washed with 0.9% saline solution and epithelial cells were dissociated by incubation with 0.1% filtered pronase (protease XIV, Sigma Chemical Co.-Aldrich, Taufkirchen, Germany) overnight at 4°C in 10 mL Ham's F12-DMEM 1/1 (Invitrogen, Karlsruhe, Germany). The cell suspension was washed three times and resuspended in 5 mL of medium containing 2% Ultroser G (Cytogen GmbH, Sinn, Germany) and plated on collagen-coated tissue flasks. Culture medium was replaced three times per week. After ~3 weeks, cells reached confluency. The collagen gel was resolved with collagenase type IV (200 U/mL; Worthington Biochemical Corporation, St. Katharinen, Germany), and the cell sheet was disintegrated with a cell scraper. After washing, the cells were resuspended in 10 mL of medium (as described above) and cultured in uncoated low attachment T25 culture flasks. To establish spheroid cultures, the flask was placed on a rotary shaker (80 rpm) and incubated at 37°C for 14 days. After 24 h, the medium was switched to Ham's F12-DMEM 1/1 supplemented with 10% NU-Serum (Schubert and Weiss GmbH, Muenchen, Germany) and replacement was carried out every second day. A total of 8 time points were isolated (day 0, 2, 4, 6, 8, 10, 12, 14). Spherois were droped on slides, dried at room temperature and stored at -80°C until high-resolution immunofluorescence microscopy analyses were performed.

Supplemental References

1. Wang, K., Li, M., and Hakonarson, H. (2010). ANNOVAR: functional annotation of genetic variants from high-throughput sequencing data. Nucleic acids research 38, e164.
2. Richards, S., Aziz, N., Bale, S., Bick, D., Das, S., Gastier-Foster, J., Grody, W.W., Hegde, M., Lyon, E., Spector, E., et al. (2015). Standards and guidelines for the interpretation of sequence variants: a joint consensus recommendation of the American College of Medical Genetics and Genomics and the Association for Molecular Pathology. Genetics in medicine : official journal of the American College of Medical Genetics 17, 405-424.
3. Hoben, I.M., Hjeij, R., Olbrich, H., Dougherty, G.W., Nothe-Menchen, T., Aprea, I., Frank, D., Pennekamp, P., Dworniczak, B., Wallmeier, J., et al. (2018). Mutations in C11orf70 Cause Primary Ciliary Dyskinesia with Randomization of Left/Right Body Asymmetry Due to Defects of Outer and Inner Dynein Arms. American journal of human genetics 102, 973-984.
4. Hjeij, R., Onoufriadis, A., Watson, C.M., Slagle, C.E., Klena, N.T., Dougherty, G.W., Kurkowiak, M., Loges, N.T., Diggle, C.P., Morante, N.F., et al. (2014). CCDC151 mutations cause primary ciliary dyskinesia by disruption of the outer dynein arm docking complex formation. Am J Hum Genet 95, 257-274.
5. Boldt, K., van Reeuwijk, J., Lu, Q., Koutroumpas, K., Nguyen, T.M., Texier, Y., van Beersum, S.E., Horn, N., Willer, J.R., Mans, D.A., et al. (2016). An organelle-specific protein landscape identifies novel diseases and molecular mechanisms. Nat Commun 7, 11491.